Summer 2009

Spatial normalization of diffusion models and tensor analysis

Madhura Aditya Ingalhalikar
University of Iowa

SPATIAL NORMALIZATION OF DIFFUSION MODELS AND TENSOR ANALYSIS

by

Madhura Aditya Ingalhalikar

An Abstract

Of a thesis submitted in partial fulfillment of the
requirements for the Doctor of Philosophy
degree in Biomedical Engineering
in the Graduate College of
The University of Iowa

July 2009

Thesis Supervisor: Associate Professor Vincent A. Magnotta

ABSTRACT

Diffusion tensor imaging provides the ability to study white matter connectivity and integrity noninvasively. The information contained in the diffusion tensors is very complex. Therefore a simple way of dealing with tensors is to compute rotationally invariant scalar quantities. These scalar indices have been used to perform population studies between controls and patients with neurological and psychiatric disorders. Implementing the scalar values may reduce the information contained in the whole tensor. A group analysis using the full tensors may give better estimate of white matter changes that occur in the diseased subjects. For spatial normalization of diffusion tensors, it is necessary to interpolate the tensor representation as well as rotate the diffusion tensors after transformation to keep the tensors consistent with the tissue reorientation. Existing reorientation methods cannot be directly used for higher order diffusion models (e.g. q-ball imaging). A novel technique called gradient rotation is introduced where the rotation is directly applied to the diffusion sensitizing gradients providing a voxel by voxel estimate of the diffusion gradients instead of a volume of by volume estimate. The technique is validated by comparing it with an existing method where the transformation is applied to the resulting diffusion tensors. For better matching of diffusion tensors a novel multichannel registration method is proposed based on a non-parametric diffeomorphic demons algorithm. The channels used for the registration include T1-weighted volume and tensor components. A fractional anisotropy (FA) channel is used for defining the contribution of each channel.

Including the anatomical data together with the tensors, allows the registration to accurately match the global brain shape and the underlying white matter architecture simultaneously. Using this multichannel registration framework, 9 healthy controls and 9 patients of Schizophrenia were spatially normalized. For the group analysis, the tensors were transformed to log-euclidean space. Linear regression analysis was performed on the log transformed tensors. Results show that there is a significant difference in the anisotropy between patients and controls especially in the parts of forceps minor, superior corona radiata, anterior limb of internal capsule and genu of corpus callosum. The results were compared to standard FA analysis as well as GA analysis.

Abstract Approved: _____
Thesis Supervisor

_____
Title and Department

_____
Date

SPATIAL NORMALIZATION OF DIFFUSION MODELS AND TENSOR ANALYSIS

by

Madhura Aditya Ingalhalikar

A thesis submitted in partial fulfillment of the
requirements for the Doctor of Philosophy
degree in Biomedical Engineering
in the Graduate College of
The University of Iowa

July 2009

Thesis Supervisor: Associate Professor Vincent A. Magnotta

Graduate College
The University of Iowa
Iowa City, Iowa

CERTIFICATE OF APPROVAL

PH.D. THESIS

This is to certify that the Ph.D. thesis of

Madhura Aditya Ingalhalikar

has been approved by the Examining Committee for the thesis requirement for the Doctor of Philosophy degree in Biomedical Engineering at the July 2009 graduation.

Thesis Committee: _____
Vincent A. Magnotta, Thesis Supervisor

_____
Joseph M. Reinhardt

_____
Daniel Thedens

_____
Edwin Dove

_____
Jinsuh Kim

_____
Andrew L. Alexander

In the memory of my father Dr. Vishwas B. Joshi

ACKNOWLEDGEMENTS

Firstly, I would like to express my deep gratitude to my adviser Dr. Vincent Magnotta for his incessant support through my PhD years. He made each problem easy through the discussions we had and his patience to explain thoroughly. I would also like to thank Dr. Jinsuh Kim, who always came up with innovative ideas and appreciation for what I did. I am indebted to Dr. Andrew Alexander from University of Wisconsin at Madison, who always provided invaluable advice on my research project.

I never would have been able to have finished the document you are now reading were it not for the immense love and support of my family: My father Dr. Vishwas Joshi who passed away in 2005, had set me an example for hardwork, devotion and dedication. My mother Mrs. Manjiri Joshi who always helped me through understanding mathematical concepts. My husband Aditya who always supported me in what I did and sacrificed a lot for me.

I would also like to mention all my close friends: Wen Li, Shruti Apte, Madhuparna Roy, Meenal Kashikar and Prem Ramakrishnan who have supported me through thick and thin during my PhD years at Iowa.

Finally, I would like to thank for the financial support provided for this work by grants NIH MH62015 and NS050568.

TABLE OF CONTENTS

LIST OF TABLES

LIST OF FIGURES

CHAPTER 1
INTRODUCTION

1.1 Motivation

Magnetic resonance diffusion tensor imaging provides an exquisitely sensitive probe of tissue microstructure. Owing to the microscopic length scale of diffusion in biological tissues, diffusion imaging can reveal histological architecture irresolvable by conventional magnetic resonance imaging methods [68] [69]. It is common to perform group analysis of diffusion tensor data based on rotationally invariant scalar indices like fractional anisotropy (FA), relative anisotropy (RA), etc. All of the subjects for the study are mapped to a common coordinate system, often defined by an atlas image. The transformation between the space of the acquired diffusion weighted images and the atlas space is defined via an image registration procedure. The resulting transformation is then applied to the scalar images where the voxel values are interpolated into the space of atlas image using conventional techniques such as linear interpolation.

Using scalar indices for population based analysis of diffusion data may reduce the statistical power and cannot detect subtle white matter changes. Potentially, spatial normalization and analysis of full tensors can maximize the power of diffusion tensor imaging.

In this thesis, a novel method for spatial normalization of diffusion tensors has been developed. The method is generalized such that it can be used for other high

order diffusion models. The first part describes a novel method for reorientation of diffusion models after a transformation is applied. In the next part, a multichannel diffeomorphic demons registration algorithm is introduced for tensor matching. Finally, a population study consisting of Schizophrenia patients is performed. The analysis is performed using linear regression on tensors transformed to log-euclidean space.

1.2 Background

The human brain consists of more than 100 billion neurons and hence is counted to be the most complex structure of our body. The complexity of the brain could be found in such neural networks which have a versatile computational architecture [37].

Description of the brain architecture has been an area of vast research for decades. Before the evolution of imaging techniques, different neuroanatomical methods were applied to study the brain architecture. In the early twentieth century, techniques were based on dissecting cadaver brains. These experiments had to be performed very carefully with immense neuroanatomical knowledge and experience. The disadvantage of the method was that it nearly impossible to study a single white matter tract. In 1960's, the use of cellular transport mechanisms was applied to detect the connectivity between the nerve cells. A tracer was injected in a particular brain region, which would then travel via axons into connected brain areas [9]. Barriers remained for studying human brain connectivity since the tracing mechanism was confined for use on living animals.

A new tract tracing method was introduced in 1970's, which could be applied to human cadaver brains. This method was based on the process of degeneration due to a nerve cell injury. The degeneration includes the axon, myelin sheaths and synapses. The process is called the Wallerian degeneration. The fiber tracts could be visualized by staining degeneration products [9].

Methods like electron microscopy, confocal laser scanning microscopy were implemented to learn the brain micro-structure. These techniques provide more information about the morphology of the nerve fiber at some particular points in the brain. Quantitative aspects were considered in stereological studies of the brain white matter. Factors like the volume of white matter, total length of nerve fibers, quantity of fibers located in a particular tract, etc. could be estimated. This was achieved by sampling the white matter sections manually, taking measurements and using statistical approximations [79].

In the past 15-20 years the use of imaging techniques to study the brain structure and function has increased rapidly. Magnetic resonance imaging (MRI) techniques, together with the advancement in image acquisition methods have expanded utilization in imaging of the brain. These tools have allowed a greater understanding of normal brain anatomy and function as well as changes associated with aging and disease pathology.

1.3 Neural Anatomy

Neurons are physical structures in the nervous system that transmit information through electrical excitation. In general, neurons are composed of 3 basic parts:

(a) Cell body or soma, (b) Axons, and (c) Dendrites. The cell body is the central part of neuron that contains the nucleus where protein synthesis occurs. The nucleus ranges from 3 to 18 micrometers in diameter. The dendrites have many branches that looks similar to a tree and are responsible for receiving signal and conducting it to the cell body. Axons are long cable like structures that transmit information away from the cell [34]. Axons lengths can vary with the longest one's being about 3-4 feet in length, extending from middle of the spine to the feet. Many neurons have only one axon, which usually undergo extensive branching, enabling communication with many target cells. The part of the axon where it emerges from the soma is called the axon hillock. Axons and dendrites in the central nervous system are typically only about one micrometer thick, while some in the peripheral nervous system are much thicker. Many neurons have insulating sheaths of myelin around their axons. The sheaths are formed by oligodendrocytes in the central nervous system. The sheath enables the signal to travel faster than in unmyelinated axons of the same diameter, while using less energy. The myelin sheath in peripheral nerves normally runs along the axon in sections about 1 mm long, punctuated by unsheathed nodes of Ranvier which contain a high density of voltage-gated ion channels [34]. Figure 1.1 shows a typical neuronal structure.

The information flow in a neuron is directional. The incoming signals are integrated, and if the summed signal is large enough, an outgoing signal, or action potential, is generated.

The mobility of water to diffuse across tracts with myelinated boundaries is

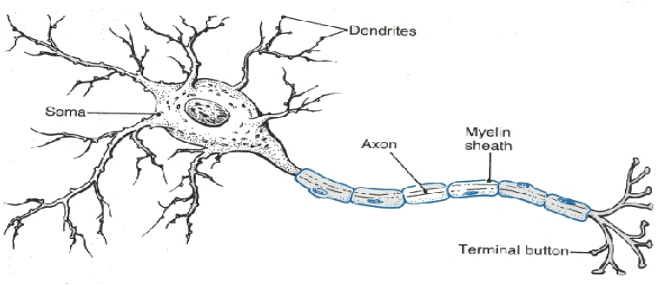

Figure 1.1: Typical neuron

restricted, causing water to diffuse anisotropically in greater amounts in directions parallel to fiber tracts and lesser amounts of diffusion in perpendicular directions.

1.4 Magnetic Resonance Imaging

Magnetic Resonance Imaging (MRI) is an imaging technique that is based on the principles of nuclear magnetic resonance (NMR), a spectroscopic technique used by scientists to obtain microscopic chemical and physical information about molecules [36]. Felix Bloch and Edward Purcell discovered the phenomenon of magnetic resonance in 1946. NMR is achieved by exciting nuclei in an externally applied magnetic field. In 1973, Lauterber used a technique called backprojection which he borrowed from computerized x-ray tomography, and produced an image of a pair of test tubes immersed in a vial of water [47]. In 1977, Peter Mansfield developed a magnetic field gradient scheme called echo-planar imaging (EPI) which did not require repeated excitation-sampling cycles, effectively reducing the required imaging time [59]. Since then Magnetic Resonance Imaging (MRI) has been used in many

biomedical, chemical and engineering applications.

1.4.1 Nuclear Magnetic Resonance

Subatomic particles such as protons have the quantum mechanical property of spin. Nuclear spin is the term often used to represent this total angular momentum of a nucleus. To exhibit the property of magnetic resonance, the nucleus must have a non-zero value of the spin angular momentum. A characteristic of a nucleus is that with an even mass number, it has integer spin (I = 0, 1,. . .), and a nucleus with an odd mass number has half-integer spin (I = 1/2 ,3/2, ..). The spin angular momentum of a nucleus with a spin number 1/2 has two energy states (+1/2, and -1/2). The particle can undergo transition between the two energy states by absorbing a photon. When the spins are placed in a strong external magnetic field they precess around an axis along the direction of the field. The angular frequency of the precession is called as the Larmor frequency ω given by equation 1.1 where γ is the gyromagnetic ratio of the particle and B is the magnetic field strength.

$$\omega = \gamma B \tag{1.1}$$

In an ensemble of nuclei, all the magnetic moments μ add up to give a net magnetization M as given in equation 1.2.

$$M = \sum_i \mu_i \tag{1.2}$$

When the ensemble is placed in a magnetic field, the quantization of magnetic

moments results in parallel and antiparallel alignment [36]. At room temperature, the number of spins in the parallel alignment, N^+, slightly outnumbers the number in the upper level, N^-. The population ratio is given by the Boltzmann's number in equation 1.3. E is the energy difference between the spin states; k is Boltzmann's constant, 1.3805x10-23 J/Kelvin; and T is the temperature in Kelvin. This population difference causes the longitudinal magnetization (M_z).

$$\frac{N^+}{N^-} = e^{-\frac{E}{kT}} \tag{1.3}$$

When a radio frequency (RF) pulse matching the Larmor frequency is applied, it alters the state of the individual magnetic moments. The RF signal makes the magnetic moments precess in coherent phase, as well. A transverse magnetization (M_{XY}) is produced due to this in-phase precessing that rotates at the Larmor frequency.

As far as medical applications are concerned, the proton (^1H) is of most interest, because of its high natural abundance.

The time taken to recover the longitudinal magnetization is called as T_1 process. The loss of phase coherence in the transverse plane is called as T_2 relaxation. Because of the magnetic field inhomogeneity, the T_2 decay time is shortened and known as T_2^*. The nuclear magnetization M is represented by using Bloch equations. In the rotating frame and in the absence of any radiofrequency (RF) field the Bloch equation is given by equation 1.4. M is the magnetization vector, γ is the gyromagnetic ratio, *r(t)* is the spin position as a function of time *t*, *g(t)* is the applied magnetic field gradient, T_2 is the spin-spin relaxation time.

$$\frac{dM}{dt} = \gamma r(t) g(t) - \frac{M}{T_2} \tag{1.4}$$

1.4.2 Image Reconstruction

In order to create the MR images, a gradient magnetic field is applied. The gradient magnetic field modifies the frequency of precession. The Larmor frequency is dependent on the position x and given by equation 1.5. The result is a spectrum of frequencies based on the location where the amplitude indicates the nuclear abundance.

$$\omega(x) = \gamma(B + G(x)) \tag{1.5}$$

The image reconstruction procedure consists of applying slice selection gradient, phase encoding and frequency encoding gradients. The slice selection pulse is applied at the same time as the RF pulse and is perpendicular to the slice plane. The phase encoding is next applied in the direction of one of the sides of the slice plane. The frequency encoding is applied during readout and is along the other direction of the slice plane. It should be noted that the gradient magnetic fields vary the main magnetic field in the direction of this main magnetic field.

The free induction decays must be Fourier transformed to obtain an image or picture of the location of spins. The signals are first Fourier transformed in one direction to extract the frequency domain information and then in the phase encoding direction to extract information about the locations in the phase encoding gradient

direction [36].

1.5 Diffusion Tensor Imaging (DTI)

1.5.1 Diffusion

Although water appears static to the naked eye, at the molecular level, water molecules are in constant random motion. This random movement is caused by the thermal agitation of water molecules and is named 'Brownian motion'. In tissues containing large number of fibers, e.g. muscle tissue and brain white matter, the motion of water molecules is restricted resulting in preferential diffusion parallel to the fibers as compared to perpendicular to the fibers. The path of the water molecule therefore reflects the structure of its microscopic environment in fibrous tissues [49]. Diffusion tensor magnetic resonance imaging (DT-MRI) measures the movement of hydrogen atoms in these diffusing water molecules. These measurements are then utilized to understand the white matter fiber architecture. In an unconstrained environment, displacement of diffusing particles is equal in all directions. This type of diffusion is called as isotropic diffusion. Measurement of diffusion is based on Einstein's equation which states that the mean-square displacement is proportional to the time that the particles diffuse.

$$r^2 = 6Dt \tag{1.6}$$

In equation 1, r is the displacement, D is the diffusion constant and t is the diffusion time. The value of 6 is introduced to account for the three dimensional nature of the motion [90].

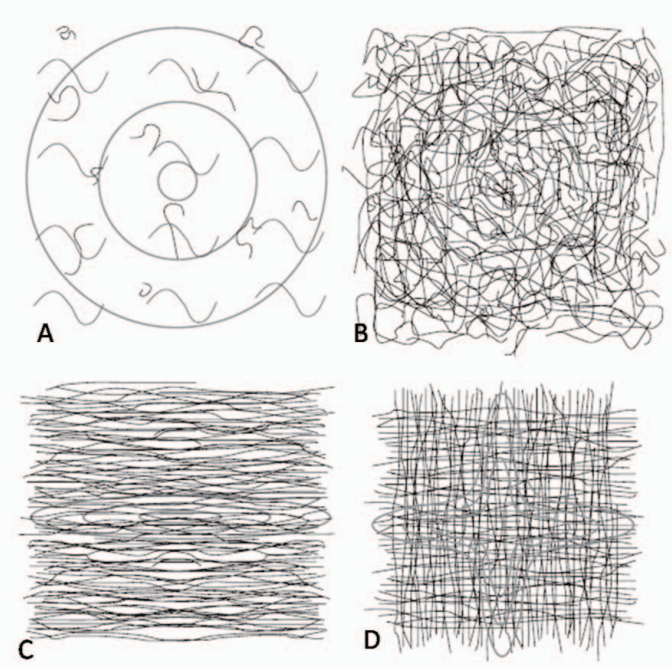

Figure 1.2: Schematic diagrams four microstructures found in the brain. The black lines are barriers to the movement of water molecules. The contours show the expected shape of probablity density function in each tissue. (A) shows a fluid-filled region. (B) shows isotropic grey matter. (C) and (D) show white matter with one and two dominant fiber orientations, respectively

The brain has a complex architecture of grey-matter areas connected by white matter fibers.The microstructures of the brain tissues limit the random motion of the water molecules resulting in restriction of total amount of diffusion. Figure 1.2 [5] shows schematic diagrams of four different microstructures that appear in brain tissue together with contours of the probablity density function that we expect to observe within each kind of tissue. Some regions of the brain, such as the ventricles, contain mostly cerebro-spinal fluid (CSF) and Figure 1.2(A) depicts such a fluid-filled region. Figure 1.2(B) depicts the gray matter regions where the diffusion function is isotropic. The brain white matter is organized in bundles of myelinated axonal fibers running in parallel and therefore the diffusion in the direction of the fibers is faster than the perpendicular direction [49]. This type of directionally dependent diffusion is termed as anisotropic diffusion and shown in figure 1.2(C). Complex microstuctures also appear in the white matter. Figure 1.2(D) shows orthogonally crossing fibers.

1.5.2 Diffusion Weighted Imaging (DWI)

A typical MR spin-echo image acquisition scheme is used with magnetic field gradients of equal magnitude that are applied before and after the 180^0 refocusing pulse. The pulse sequence is called as pulsed gradient spin echo (PGSE).The sensitivity to the diffusion of water is caused by the strong magnetic gradients. Figure 1.3 shows the pulse sequence for Diffusion Weighted Imaging (DWI). The 90^0 pulse excites the spins. The diffusion gradient of magnitude g and time duration δ is then applied. The gradient gives a phase to the spins proportional to their location. The refocusing pulse inverts the direction of the spins. The second gradient is applied

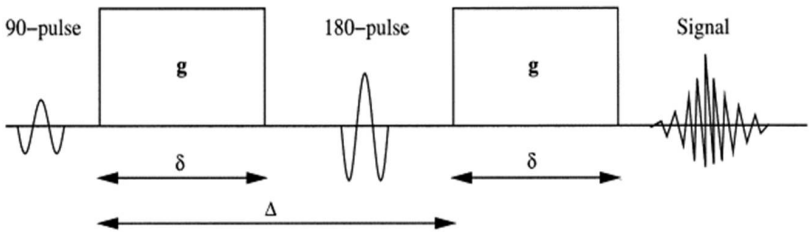

Figure 1.3: DWI Pulse Sequence

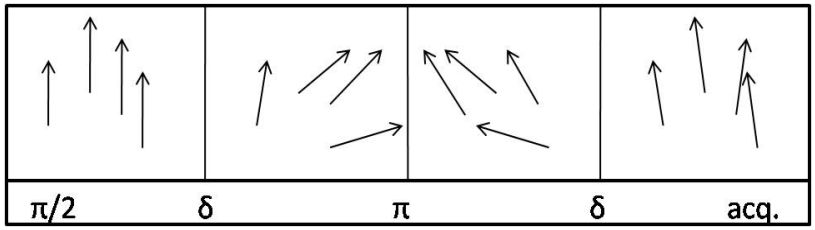

Figure 1.4: Schematic diagram of spin phase distribution for Pulsed Gradient Spin Echo sequence.

after time duration Δ and is equal to the first gradient with respect to magnitude and time. Because of the movement of water molecules between the two gradients, the rephasing is not complete, resulting in a signal loss. Figure 1.4 shows the spin diagram at every stage. Generally, an echo planar sequence (EPI) is employed for DWI to reduce the acquisition time.

The Bloch equations 1.4 were modified by Torrey to include the effects of molecular diffusion and flow to give the Bloch-Torrey equation [81]. The Bloch-Torrey equation was solved by Stejskal and Tanner [76]. The simplified version of the Stejkal-Tannar equation is given in 1.7. This equation allows us to relate the observed

diffusion signal to the underlying diffusion coefficient assuming that the diffusion is purely Gaussian.

$$S = S_0 e^{-bD} \tag{1.7}$$

Where, S is the measured signal, S_0 is the signal without diffusion weighting gradients and b is the diffusion weighting. D is the diffusion constant and is termed as apparent diffusion coefficient (ADC). The b-value depends upon strength and duration of the gradient and also the time duration between two pulsed gradients as described in equation,

$$b = \gamma^2 \delta^2 [\Delta - \frac{\delta}{3}] g^2 \tag{1.8}$$

where γ is the gyromagnetic ratio, δ is the gradient pulse width, Δ is the time between gradient pulses, g is the strength of the diffusion gradient pulses.

Since the process of diffusion is of the order of micrometers, DTI can be called as a macroscopic model for microscopic process [90]. The overall effect observed in a diffusion tensor image voxel of several cubic millimeters reflects, on a statistical basis, a Gaussian displacement distribution of the water molecules present within each voxel [49].

1.5.3 Diffusion Tensor

In tissues like brain gray matter, it is usually sufficient to characterize the diffusion characteristics with the apparent diffusion coefficient (ADC). However, in white matter where the measured diffusivity is known to depend upon the orientation of the tissue, no single ADC can characterize the orientation-dependent water mobility

in these tissues [11]. Hence, a second rank tensor is used as a model for characterizing diffusion as a three-dimensional process. The model is called a diffusion tensor and is represented by a 3 x 3 symmetric tensor [68].

$$(D) = \begin{bmatrix} D_{xx} & D_{xy} & D_{xz} \\ D_{yx} & D_{yy} & D_{yz} \\ D_{zx} & D_{zy} & D_{zz} \end{bmatrix} \tag{1.9}$$

Since diffusion is encoded in the MRI signal by using magnetic field gradient pulses, only molecular displacements occurring along the direction of gradient are visible [50]. Therefore in order to compute the diffusion tensor D, measurements must be made with the diffusion weighting gradients in atleast six non-collinear directions and as well as with no diffusion weighting. Therefore, diffusion tensor MRI requires a minimum of seven MRI measurements. Most diffusion-tensor MRI sequences acquire more than the minimum seven measurements to reduce the effects of noise. The number of gradient directions used is distributed uniformly over a sphere. Figure 1.5 [49] shows the sampling of directions.

In general, the diffusion tensor D depends on particle mass, the structure of the medium, and temperature [15]. In DTI, the particle mass of water molecules and the temperature at which measurements are conducted is assumed constant. This assumption allows for the diffusion tensor in DTI to be interpreted solely in terms of local anatomical structure.

Geometrically, a symmetric second rank tensor can be viewed as an ellipsoid

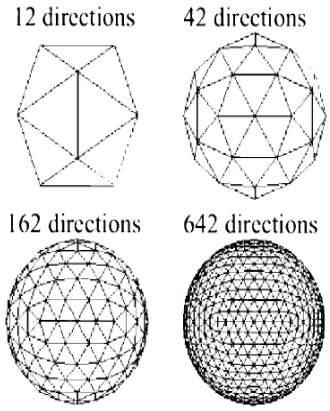

Figure 1.5: Sampling of diffusion directions. Conventionally, diffusion sensitizing encoding directions are set to be uniformly distributed and a single diffusion weighting factor is used for all directions.

characterized by the eigenvalues λ_1, λ_2, λ_3 and their corresponding eigenvectors v_1, v_2, v_3 (Equation 1.10) [50]. The eigenvalues describe the shape of the ellipsoid, while the eigenvectors express the orientation of the ellipsoid. The principle axis is the eigenvector corresponding to the highest eigenvalue. In voxels where λ_1 is much larger than λ_2 and λ_3, the orientation of the primary eigenvector, v_1, defines the orientation of white matter within each voxel. Figure 1.6 shows the diffusion tensor. The axes of the ellipsoid are oriented in the direction of the diffusion tensor eigenvectors and have lengths proportional to the square-root of the diffusion tensor eigenvalues.

$$(D) = \begin{bmatrix} D_{xx} & D_{xy} & D_{xz} \\ D_{yx} & D_{yy} & D_{yz} \\ D_{zx} & D_{zy} & D_{zz} \end{bmatrix} = E^T \begin{bmatrix} \lambda_1 & 0 & 0 \\ 0 & \lambda_2 & 0 \\ 0 & 0 & \lambda_3 \end{bmatrix} E \tag{1.10}$$

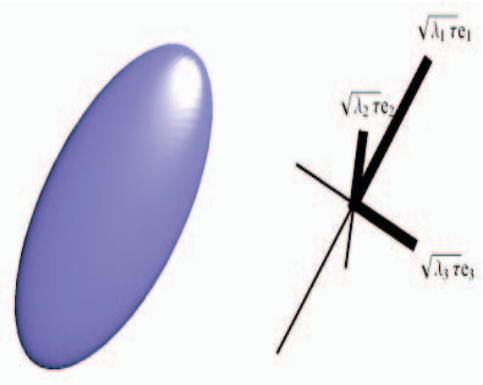

Figure 1.6: The ellipsoid representing the tensor structure. The eignevalues and eignevectors define the shape and the orientation respectively

In case of purely isotropic diffusion, $\lambda_1 \approx \lambda_2 \approx \lambda_3$. Two different cases of anisotropic diffusion can be possible. First one is called linear case or prolate case where $\lambda_1 >> \lambda_2 \geq \lambda_3$ and another one is the planar case or oblate case where $\lambda_1 \approx \lambda_2 > \lambda_3$. Figure 1.4 illustrates all 3 cases.

1.5.4 Diffusion Anisotropy Indices

Various rotationally invariant scalar measures of the diffusion tensor can be extracted in order to summarize the geometric properties of the tensor eigensystem, facilitate visualization on a two-dimensional plane or, enable statistical comparisons

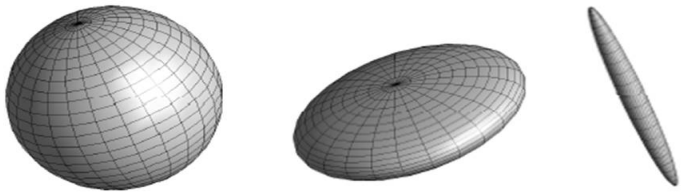

Figure 1.7: 3 cases of diffusion: Isotropic (Depicted by a sphere), Anisotropic Planar or disc type or oblate and Anisotropic Linear or cigar shaped or prolate

between subjects or groups of subjects. While many such scalar measures have been defined in the literature we will present those which that care commonly used and also referred in this thesis: the tensor trace, the fractional anisotropy, the relative anisotropy and the skewness. Figure 1.8 shows some of the scalar images.

1.5.4.1 Tensor Trace

The trace, T, of the diffusion tensor is simply the sum of eigenvalues. The trace is proportional to the mean squared displacement of water molecules and thus indicates the mobility of water molecules within each voxel.

$$T = \lambda_1 + \lambda_2 + \lambda_3 \tag{1.11}$$

1.5.4.2 Fractional Anisotropy

The FA measures the fraction of the value of the tensor that can be attributed towards anisotropic diffusion. The FA values are normalized between 0 and 1 where 0 is the isotropic case ($\lambda_1 = \lambda_2 = \lambda_3$) and 1 is purely anisotropic case ($\lambda_1 =$ c and λ_2

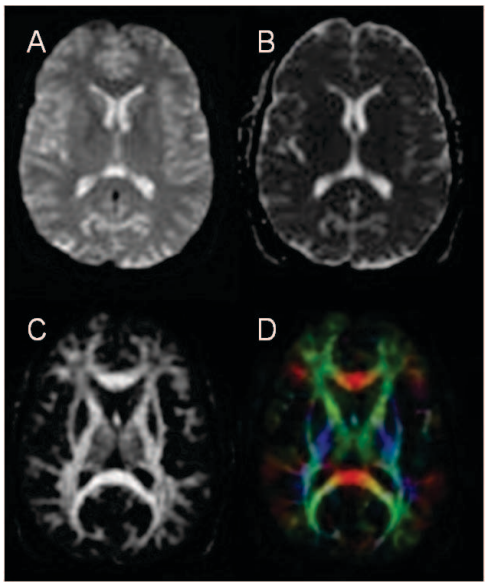

Figure 1.8: Axial slice showing (A) T2 weighted image (B) Trace image (C) Fractional Anisotropy (D) Color coded Fractional Anisotropy based on direction of fibers.

$= \lambda_3 = 0$).

$$FA = \sqrt{\frac{3}{2}} \frac{\sqrt{(\lambda_1 \quad \overline{\lambda})^2 + (\lambda_2 \quad \overline{\lambda})^2 + (\lambda_3 \quad \overline{\lambda})^2}}{\sqrt{\lambda_1^2 + \lambda_2^2 + \lambda_3^2}} \tag{1.12}$$

1.5.4.3 Relative Anisotropy

The RA value represents the ratio of the anisotropic part of the tensor to its isotropic part.

$$RA = \frac{\sqrt{(\lambda_1 \quad \overline{\lambda})^2 + (\lambda_2 \quad \overline{\lambda})^2 + (\lambda_3 \quad \overline{\lambda})^2}}{\sqrt{3}\overline{\lambda}} \tag{1.13}$$

1.5.4.4 Skewness

The skewness of a tensor is used to distinguish between the tensors that are prolate (cigar-like) and oblate (disc-like). For prolate tensors the skewness value is

greater than zero while for oblate tensors it is less than 0.

$$\mu = \frac{(\frac{9}{2}\sum_{i=1}^{3}(\lambda_i - \frac{1}{3}Tr(D))^3)^{\frac{1}{3}}}{\sum_{i=1}^{3}(\lambda_i^3)} \tag{1.14}$$

1.5.5 Diffusion Tractography

Fiber tracking based on diffusion tensor imaging is an approach available to non-invasively study the structure of white matter tracts. Basic DTI provides a means for determining the overall orientation of white matter bundles in each voxel by considering the principle eigenvector direction. Here, the assumptions are that the fiber architecture in every voxel is well represented by a single vector and the noise has negligible effect on the direction of principle eigenvector [50]. A number of fiber tracking algorithms have been developed since the advent of DT-MRI. Two types of approaches are prominently used for fiber tracking. The first one is streamline tractography (SLT or STT) and the second one is fast marching tractography (FMT). The SLT assumes that the direction of the principle eigenvector represents the orientation of dominant axonal tracts. A variation of the SLT is tensorline tractography (TEND) introduced by Lazar et al. The algorithm uses entire diffusion tensor to deflect the incoming vector [48]. Another technique developed by Mori et al. is the fiber assignment by continuous tracking (FACT) algorithm which alters the propagation direction at voxel boundary interfaces [60]. The fast marching algorithm developed by Parker et al. is based on the concept of level set theory [66].

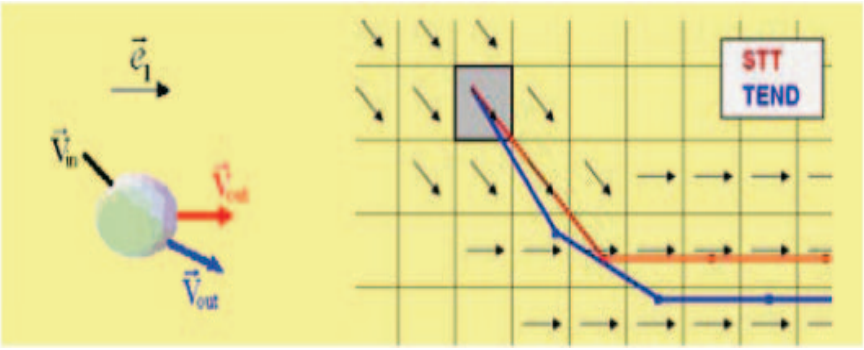

Figure 1.9: Diffusion directions followed by STL and TEND

1.5.5.1 Streamline Tractography

The conventional white matter tractography reconstructs the pathways of white matter tracts by starting from a seed voxel and tracking down the trajectory in a voxel-by-voxel manner, using an estimate of the local fiber orientation determined by the principal eigenvector in each voxel [26]. At each voxel the eigenvector corresponding to the largest eigenvalue i.e. the principle eigenvector, is aligned with the mean fiber direction in that voxel [96]. This procedure is followed until the threshold is reached. The threshold used is usually the FA value. The popular streamline tracking algorithm proposed by Basser et al. uses Euler's approximation method to solve the 3D path equation. The integrated path is connected as a path of one fiber tract [68].

The streamline tracking is the most commonly used tracking algorithm. It is easy to implement and gives good results especially where the fibers are strongly oriented in certain direction, for example, in the corpus callosum. In the regions of

fiber crossing, branching or merging the tensor data is difficult to interpret using this algorithm. Tracts tend to terminate when they encounter such ambiguous regions. Also SLT is susceptible to image noise.

The performance in the presence of noise can be improved using TEND algorithm. The algorithm uses the entire diffusion tensor to deflect the incoming vector direction as illustrated in figure 1.9. The tensor operator deflects the incoming vector towards the major eigenvector direction, but limits the curvature of the deflection, which should result in smoother tract reconstructions [48]. The tensorline tracking is smoother than other algorithms but doesn't work well if the tracts are crossing or merging.

Another algorithm known as guided diffusion tensor tractography (GTRACT) is capable of handling the fiber crossing problem correctly. The algorithm consists of four steps. The first step generates an initial guess of the fiber tracts. Forward and backward tracking is done using partial and restricted 3D graph search algorithm. The second step performs a merging operation to form fiber bundles from the forward, as well as the backward tracking. The outlier fibers are removed in this step. A guide fiber is created in the third step by considering the means after resampling the fiber bundle. The final step is to perform an improved streamline tracking where the guide fiber direction is taken into consideration [23] Figure 1.10 compares simple streamline tracking with the innovative GTRACT algorithm for the fiber crossing problem which is performed on a phantom data. It can be observed that GTRACT solves the crossover problem while SLT cannot.

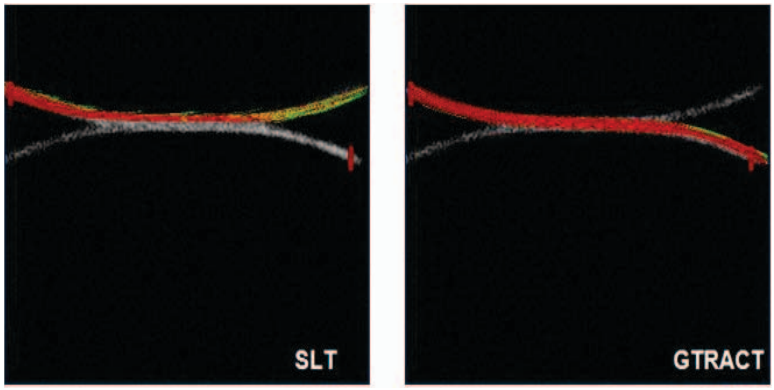

Figure 1.10: STL incorrectly tracts at the crossover while GTRACT handles the fiber tracking problem correctly

1.5.5.2 Fast Marching Tractography

This technique developed by Parker et al., utilizes orientation of the diffusion tensor to define speed of propagation of the interface or the front as shown in figure 3.7. The principles of level set theory and fast marching algorithm are implemented. Starting from a user defined seed point, the rate F at which the front propagates, is linked to the information contained in the principle eigenvector, i.e. e_1 field as shown in figure 1.11 [66]. Each iteration of the front position evolution involves determination of the rate of propagation F(r), where r is the position of any of the voxels that are candidates for being crossed by the front [25]. F(r) can be defined as a measure of voxel similarity between the neighboring voxels. The similarity is high when the principle eigenvectors of both the voxels are collinear. Hence in white matter fiber tracts the front propagation is the fastest as there is a strong coherence between the principle eigenvectors.

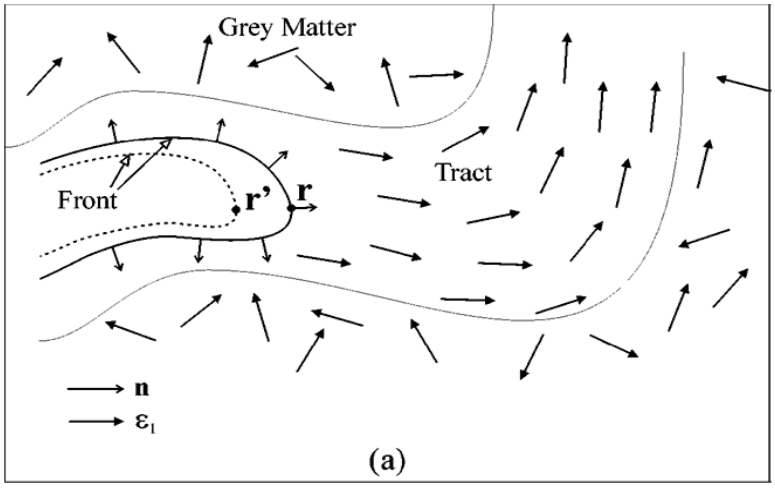

Figure 1.11: A schematic showing FMT front in the directionally coherent white matter. The coherence is lacking in the grey matter.

1.5.6 Applications of Diffusion Tensor Imaging

Diffusion Tensor Imaging (DTI) is the only modality in MRI that is unique in its ability to noninvasively visualize the white matter fiber tracts in vivo. Because of such distinctive capability of this method, it serves a number of applications.

During the acute stage of brain ischemia, water diffusion is decreased in the ischemic territory by as much as 50 percent [61]. These results were confirmed in human stroke cases and diffusion MRI is under clinical evaluation as a tool to help clinicians optimize their therapeutic approach to individual patients and to monitor patient progress [89].

Diffusion imaging has been used to evaluate brain connectivity and changes in white matter architecture during development and aging [14], [83], [74]. It has been shown that the degree of diffusion anisotropy in white matter increases during the

myelination process and hence diffusion MRI could be used to assess brain maturation in children, newborns, or premature babies [62].

It has been used to study changes in white matter associated with neurological and psychiatric diseases. Schizophrenia is the most widely investigated disorder using DTI [45], [56], [7]. Voxel based group analysis based on diffusion scalar indices is commonly performed. Neurodegenerative diseases like Alzheimer's disease, Multiple Sclerosis, leukoencephalopathy, Huntington's disease etc. are evaluated based on voxel based morphometry of the DTI data [98]. Reduced anisotropy in the left-tempero parietal regions has been observed in dyslexic adults [43].

Effects of drug abuse and alcohol abuse on the white matter architecture and density have been examined using DTI [57]. DTI has also been applied in studying brain tumor grading [44], trauma [10], hypertensive hydrocephalus [73], AIDS [22], eclampsia [72], leukoaraiosis [40] and migraine [21]. Other applications include studying the relation between structure and function [91] and as a tool to assist in computer guided surgery and treatment planning [17], [63], [28].

1.5.6.1 Diffusion tensor imaging and Schizophrenia

Schizophrenia is a serious and disabling mental disorder. It affects 1% of the population and has been shown to involve a number of brain regions. Several studies have shown changes in the structure and function of grey matter regions. Recently, white matter anomalies have also been reported in patients with Schizophrenia. In a study conducted by Lim et al, relative to controls, the patients with schizophrenia exhibited lower anisotropy in white matter, despite absence of a white matter volume

deficit [56]. Agartz et al. observed that fractional anisotropy was reduced in the splenium of the corpus callosum and in adjacent occipital white matter. In the study by Kubicki et al. they showed disruption in the white matter connectivity between the frontal and temporal lobes [45]. Although the findings are varied, there could be global and regional white matter abnormalities occuring in chronic schizophrenia. In this thesis, we have performed statistical analysis on tensors between healthy controls and patients with Schizophrenia.

1.5.7 Limitations of Diffusion Tensor Imaging

The diffusion imaging technique is prone to a number of artifacts that can severely affect its ability to provide clinically useful information. The movement of the subject inside the scanner can cause ghosting of images. Artifacts resulting from rigid body motion are the easiest to correct for, since this involves applying a uniform phase correction to an entire image [11]. Use of fast echo planar imaging and cardiac gating can aid in reducing the motion artifacts like respiratory motion, eye movement etc.

Eddy current artifacts are caused because of the rapid switching of the magnetic field gradients. Because of the eddy currents a small magnetic field is produced that causes the actual b value to be different than the assumed value and also causes geometric distortion because of the difference in the read out gradient. The eddy current artifacts can be reduced by using bipolar diffusion encoding gradients [2]. Jezzard et al. have proposed acquiring one-dimensional field maps in the read and phase encode direction for each slice and each diffusion step [38]. Another approach is

Table 1.1: Length scales of the brain tissue compared with the voxelsize

Voxel size	1.0 mm^3
Diffusion time	10^{-2}sec.
Displacement of water molecules	few μm
Diameter of Axons	mostly 10^{-6} m
Packing density of axons	10^{-11}m

to use a mutual information criterion to determine a warp that maximizes the overlap within a series of diffusion-weighted images.

Although diffusion tensor MRI is the most popular reconstruction algorithm, it has a major drawback. Diffusion tensors provide only one fibre-orientation estimate in each voxel. The diffusion occurs at a micrometer scale, while generally the resoution is such that the voxel size is between 1.0 mm^3 to 8.0 mm^3. Table 1.5.7 gives an idea of the scales. In regions where fibers cross within one voxel, the probablity density function has multiple directions. The Gaussian model has oblate ellipsoids. For a perfectly oblate Gaussian distribution, the tensor has no unique principal eigenvector. Sometimes the fibers do not cross orthogonally but at various angles. In such cases implementing the tensor model can be incorrect [5].

1.6 Diffusion Q-ball Model

A limitation posed by diffusion tensor model is that it cannot resolve intravoxel orientational heterogeneity. This is because the tensor assumes single Gaussian diffusion function in each voxel. Q space imaging (QSI) can be implemented to solve the intravoxel fiber heterogeneity by sampling the diffusion signal on a three dimensional Cartesian lattice. Sampling on three dimensional lattice is time expensive and hence

an alternative approach based on sampling on a spherical shell in diffusion wavevector space is employed [82]. The spherical sampling approach is referred as high angular resolution diffusion imaging (HARDI). A model free reconstruction scheme for HARDI has been proposed by Tuch called Q-ball imaging (QBI). The QBI reconstruction is based on a spherical tomographic inversion called the Funk Radon transform, also known as the spherical Radon transform or simply the Funk transform. The QBI has significant advantages like linearity, model independence and ability to resolve intravoxel fiber orientations. The intravoxel orientations are defined by a diffusion orientation distribution function (ODF). Tuch has shown that the Funk Radon transform of the diffusion signal is proportional to the ODF. An example of a fiber crossing region is shown in figure 1.12. In each voxel a min-max normalized ODF is shown.

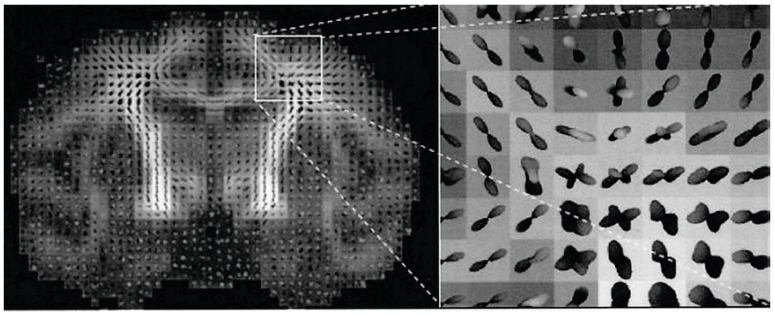

Figure 1.12: Q-Ball reconstruction using Funk-Radon Transform.

1.7 Spatial Normalization

It is common to perform group analyses of diffusion tensor data based on scalar indices (examples are FA or RA). The comparison is generally carried out using region of interest (ROI) based or voxel-based methods. ROI-based methods begin with identifying the anatomical region and are used in cases where anisotropy change is predicted in a particular region [46] [31]. While in the voxel-based methods, all the subjects are mapped to a common coordinate system, often defined by an atlas image [70]. The transformation between the space of the acquired diffusion weighted images and the atlas space is defined via an image registration procedure. The resulting transformation is then applied to the scalar images where the voxel values within the atlas space are interpolated using conventional techniques such as linear interpolation. Packages like SPM [32] or FSL [75] [93] use non-linear registration techniques to align FA data of all the subjects that is then used for group analysis. A drawback of using voxel-based method is that imperfect registration can lead to anatomical confounds.

Using only the scalar indices may significantly decrease the statistical power of the group studies in detecting subtle changes in white matter architecture. Therefore for consideration of the orientation information in diffusion image analysis, the spatial normalization can be performed directly on the diffusion tensors or any other diffusion model. Spatial normalization of tensors consists of two parts: registration of tensors with the template and reorientation of tensors to be consistent with the underlying anatomy.

A number of methods have been proposed for tensor reorientation. Xu et al (2003) implemented a method where the reorientation is computed from the spatial normalization transformation and from estimating the probability density function (PDF) of the underlying fiber orientation using a Procrustes fit [94]. Alexander et al (2001) introduced two other reorientation techniques. The first one is the finite strain model (FS) in which the final transformation is decomposed into a deformation component and a rigid rotation component. The rotation is accomplished by applying the rigid rotation component to the tensor. The second method introduced by Alexander et al. is the preservation of principal direction (PPD). In the PPD method, the rotation is computed by both the deformation as well as rotation components. For higher-order, non-linear transformations, Alexander et al. introduced a reorientation technique based on the displacement field [4]. This technique estimates a local affine model of the nonlinear transformation by computing the Jacobian of the displacement field. An appropriate rotation matrix in each voxel is then computed using either FS or the PPD method and applied to the tensor.

Registration of diffusion tensors can be performed directly or indirectly. In the indirect method, the registration is driven by a scalar quantity like FA, from which a deformation field is estimated. With the computed deformation field or transformation function, the morphology of the diffusion tensor is deformed to fit a template space. This transformation function can be either an affine transformation or a nonlinear elastic warping. Recently, some work has been done in registering the diffusion tensors directly. Alexander and Gee introduced an elastic matching

algorithm based on tensor similarity measures. Reorientation was performed using the preservation of principal direction (PPD) method after each iteration [3]. Zhang et al proposed a local affine registration algorithm using the finite strain (FS) reorientation strategy [97]. Park et al proposed a demons algorithm using tensor components with PPD reorientation [65]. Recently, Yeo et al demonstrated that including the exact FS differential in computation of the gradient resulted in better matching of tensors [95].

1.8 Tensor Analysis

DWI can be used to analyse neurological and psychiatric disorders by using population atlases of the brain. Demand for statistic based group analysis methods that can quantify the variation in brain structures has increased. A majority of the group studies to this date use scalar indices like FA and RA for analysis [31], [18]. Scalar analysis can be either performed by manual placement of region of interest (ROI) and computing the mean anisotropy within that region or on a voxel by voxel statistics after coregistrating all the subjects to one space.

Analysis on scalar images does not account for the complete information present in the tensors and requires a priori knowledge of how pathology affects the tensors [86]. A limited number of tensor based analysis tools have been developed to date. Many attempts to analyse the tensors were based on a Gaussian model of the linear tensor coefficients. One of the methods developed by Jones et al. concentrated on computing the mean median and mode of the tensor in each voxel. This was achieved using Fréchet distance concept [39]. Another vector space based methods include linear operations like principal component analysis (PCA).

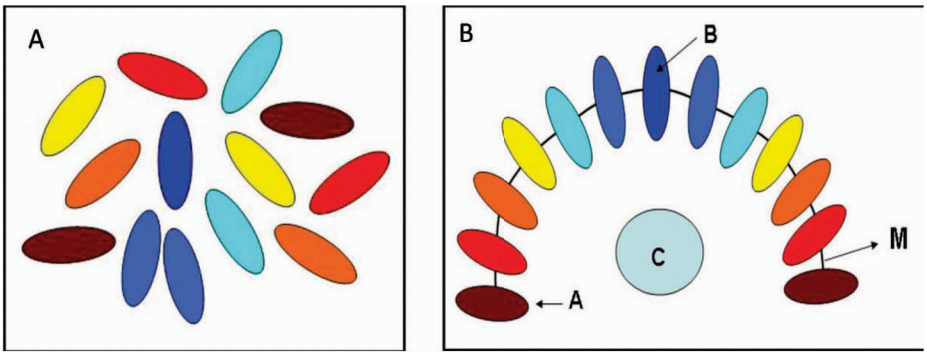

Figure 1.13: Figure shows the underlying manifold of the tensors. (A) Collection of tensors whose statistical average is to be determined. (B) The underlying manifold structure M. Linear average is given by tensor C while B gives the average on manifold

Developing methods for analysis of tensors is a complex problem since voxel based linear statistics cannot be applied directly. Diffusion tensors are symmetric positive definite matrices, they lie in a non-linear space and conventional vector space techniques like averaging, interpolation, hypothesis testing etc. cannot be performed [16] [52]. A good example of how the tensor non-linearity can affect the tensor statistics is given in figure 1.13 [86]. Although tensors might appear complex, it may have an underlying low dimensional structure.

Several groups developed a Riemannian metric framework for determining the underlying manifold of the tensor and perform geodesic analysis [29] [67] [13]. Using the affine invariant Riemannian metric on tensor spaces, the distance between two tensors A and B is given by equation 1.15.

$$dist(A,B) = log \left\| A^{\frac{1}{2}}.B.A^{\frac{1}{2}} \right\| \tag{1.15}$$

Recently, Verma et al. proposed a manifold learning technique called Isomap, that embeds the tensors in lower dimensional space that can be analysed using multivariate statistics [86].

The drawback of using the affine invariant Riemannian metrices is that they are computationally expensive. Therefore, Arsigny et al., proposed another metric called as the log-euclidean metric that is simple to use. The log-euclidean metric is a Riemannian metric and therefore preserves all the properties of the tensors. Its simplicity is such that the classical euclidean computations can be performed in matrix logarithms [8].

CHAPTER 2
METHODS

This research focuses on creating a generalized framework for spatial normalization of diffusion models. For reorientation of the diffusion models, a novel technique called gradient rotation is developed. In this method, rotations are applied to the diffusion sensitizing gradients providing a voxel-by-voxel estimate of the diffusion gradients instead of a volume of by volume estimate. We have generalized the method such that it can be used for any type of transformation. The rotation is computed from the displacement field as described by Alexander et al (2001) [4]. Since the gradients are rotated and the gradient images are warped before computing the diffusion model, we can completely eliminate the complex problem of tensor interpolation. Another advantage of the gradient rotation method is that, it can be applied to higher order diffusion models like the q-ball model and diffusion kurtosis as well as can be implemented in diffusion spectrum imaging (DSI). Kim et al (2008) have applied gradient rotation method to q-ball data effectively [41].

A multistage registration sequence is proposed for spatial normalization of tensors. The intersubject matching is carried out using a novel multichannel registration, based on non-parametric diffeomorphic image registration with demons algorithm [84]. Our approach concentrates on alignment of gray matter areas using T1-weighted image coupled with white matter matching using the diffusion tensor components. The T1-weighted image serves as a morphological signature that facilitates

to find anatomical correspondence during the registration. The coupling between the channels is based on FA values.

Finally, the complete framework is applied to 9 controls and 9 patients of Schizophrenia. All the subjects were spatially normalized with respect to the chosen template subject. Analysis was performed between groups using regression methods in log-euclidian space [55].

2.1 Gradient Rotation method

A generalized approach was implemented for transformation of the tensors via gradient rotation using FS. Any type of transformation or deformable registration represented by a deformation field is supported. After registration, the resulting transformation (T) can be expressed using a displacement field (u). A local linear transformation (F) can be described as

$$F = I + J_u \tag{2.1}$$

Where,

$$J_u = \frac{du}{dx} \tag{2.2}$$

is the Jacobian of the displacement field at each point x, and I is the identity matrix. According to the polar decomposition theorem, a non-singular deformation gradient tensor can be decomposed into the finite strain parameters of rotation and strain tensor. Therefore transformation F can be decomposed into rotation, R, and defor-

mation, U [4].

$$F = UR \tag{2.3}$$

A singular value decomposition method (SVD) is then employed to obtain the rotation tensor component, R. A local diffusion gradient at each voxel was computed using,

$$g_{rot} = R * g \tag{2.4}$$

where g is the uncorrected diffusion gradient vector and g_{rot} is the corrected local gradient vector. For any type of transformation, i.e. linear or nonlinear, based on the rotation matrix R, the gradient can be computed in each voxel. Standard interpolation techniques can then be applied when resampling each of the diffusion weighted images into the space of the target image. Following gradient correction, the tensor is computed in each voxel.

Another method for reorientation of tensors proposed by Alexander et al., is called as the preservation of principal direction (PPD) method [4]. The advantage of using the PPD method is that it takes into consideration the shear and scale components. The PPD method is described below:

Given a linear transformation matrix, F and a diffusion tensor D the PPD method proceeds as follows:

1. Compute unit eigenvectors e_1, e_2, e_3 of D.

2. Compute unit vectors n_1 and n_2 in the direction of Fe_1 and Fe_2 respectively.

3. Compute a rotation matrix R_1 that maps e_1 onto n_1. A secondary rotation about n_1 is required to map e_2 from its position after the first rotation, R_1e_2 to the n_1-n_2 plane.

4. Find projection $P(n_2)$ of n_2 onto a plane perpendicular to R_1e_1. $P(n_2) = n_2 - (n_2.n_1).n_1$

5. Compute a second rotation R_2 that rotates R_1e_2 onto a unit vector in the direction of $P(n_2)$.

6. Set $R = R_2R_1$ and reorient D using equation 2.8.

Similar to the PPD method proposed by Alexander et al., the gradient rotation method described above can be extended to take into account the scale and shear components when estimating the rotation matrix. To extend the gradient rotation method, a principal components analysis (PCA) is used to compute the covariance matrix C as shown in equation 2.5.

$$C = \frac{1}{n}\sum_{i=0}^{n-1} d_i d_i^T \tag{2.5}$$

where

$$d_i = D * g_i \tag{2.6}$$

In the above equations, n is the number of gradient directions while D is the apparent diffusion coefficient and g_i is the gradient vector [24]. The covariance matrix (C) is decomposed into eigensystem as shown in equation (2.7) where, Λ is a

diagonal matrix with eigenvalues of C while E is a matrix made of three eigenvectors. These matrices are employed in the gradient rotation PPD method as described by Alexander et al (2001). The rotation matrix calculated from the PCA analysis is applied to the gradients using equation (2.4).

$$C = E^T \Lambda E \tag{2.7}$$

A multi-step evaluation study was conducted to compare the gradient rotation methods to the traditional tensor rotations methods. First, a within subject evaluation was carried out by imaging subjects multiple times with different head positions. Next, all subjects were registered to a common coordinate system. The various methods were compared using a variety of metrics as described in the subsequent section.

2.1.1 Experiment for Validation of Gradient Rotation

Five healthy subjects underwent a multiple sequence MR imaging study that included T1-weighted, T2-weighted and diffusion tensor imaging after informed consent was obtained in accordance with the Institutional Review Board at the University of Iowa. The data was acquired on a 3T Siemens TIM Trio scanner using a 12 channel head coil. The T1-weighted sequence was collected using a coronal 3D magnetization prepared rapid gradient echo (MP-RAGE) sequence with the following parameters: TR/TE=2530/3.04 ms, TI=800 ms, flip angle=10, matrix=256x256x220, FOV=256x256x220 mm. Diffusion tensor imaging was performed using a dual spin-echo, echo-planar sequence with the following parameters: TR/TE=8700/86 ms,

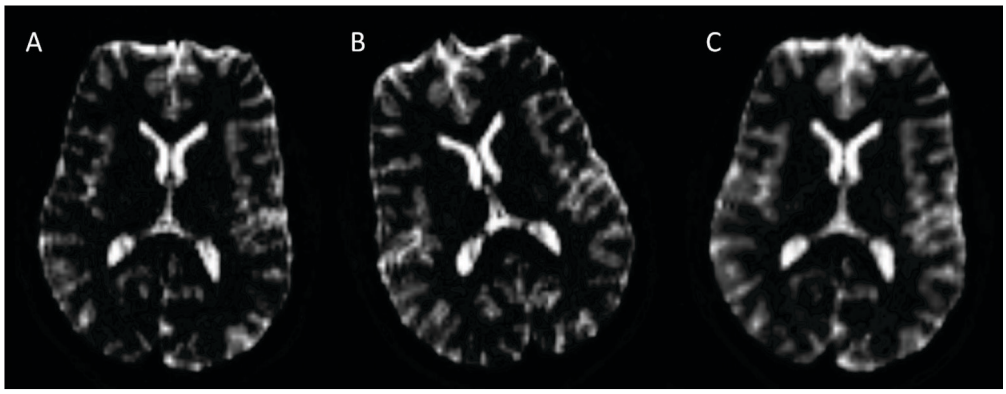

Figure 2.1: b=0 image collected for a single subject. A. Normal head position and B. Head tilted by approximately 30 degrees.

matrix=128x128, FOV=256x256mm, slice thickness =2.0mm, b-value=1000s/mm^2, number of directions=64. The DTI sequence was repeated to obtain two different datasets. During the second sequence, subjects were told to turn their head sideways by approximately 30 degrees. The purpose of having two diffusion scans for each subject was to test the capability of our method between these two datasets. Figure 2.1 (A and B) show an example of the two b=0 images collected for the same subject.

The DICOM diffusion-weighted image data were first converted into nrrd format(http://teem.sourceforge.net/nrrd/index.html). During this process, the Siemens mosaic images were unpacked and the gradient directions converted into the subject frame of reference. The diffusion weighted images were then corrected for motion and eddy current artifacts using the GTRACT software [23]. To achieve this, the b=0 image served as a reference image and all other diffusion weighted images were matched using a mutual information metric [87] and subsequently aligned by an affine trans-

formation. These motion correction parameters were also used to adjust the diffusion sensitizing gradient orientation.

The second dataset b=0 image (head turned -Figure 2.1B) was co-registered with the first dataset b=0 image (head in neutral position - Figure 2.1A) using a rigid body transformation. For this analysis, the image with the head in the neutral position was considered the fixed image and the image with the head rotated by 30 degrees was considered the moving image. A mean square error metric was used and the registration was initialized using the center of mass from the fixed and moving images. For validation of gradient rotation method, a rigid body registration was used since this would theoretically be sufficient to achieve alignment between the intrasubject datasets ignoring the effect of susceptibility artifacts. Figure 2.1C shows the head turned image after warping with the deformation field.

A displacement field was computed from the resulting rigid body transform. A rotation matrix (R) at each voxel was calculated from the displacement field using equations (2.1) and (2.2). The gradient vector for each voxel was corrected by using equation (4). The diffusion tensor field was then estimated using a least squares fitting method with background thresholding at an intensity level of 80 on the b = 0 image. To apply the tensor reorientation method, the tensor field was first computed and then tensor was rotated voxel by voxel using equation (2.8) where R is computed using equation (2.3).

$$D' = RDR^T \tag{2.8}$$

The resultant reoriented tensors were visually compared with the corresponding tensor

representation obtained with neutral head position. Based on initial observations, it was determined that the normal head orientation data was substantially more noisy as compared to the reoriented data due to an implicit low pass filtering characteristics of the linear interpolation during the resampling process. To account for this difference, a diffusion weighted data in the normal head orientation was filtered using low pass Gaussian filter with a sigma of 1mm. The sigma value was chosen empirically to match the smoothing from resampling of the resulting tensors.

To evaluate the reorientation strategies, three different quantitative measures were utilized. The first method computes the angle in each voxel, between the principal direction (PD) of the reference image and PD in the transformed image. The resulting angle signifies the relative orientation between the reoriented and reference image. The angular separation (θ) can be computed from the dot product as shown in equation (2.9).

$$\theta = cos^{-1}\left\{\frac{e_{a1}.e_{b1}}{|e_{a1}| * |e_{b1}|}\right\} \tag{2.9}$$

Since PD's are prominent in white matter regions that are prolate i.e. $\lambda_1 >> \lambda_2 > \lambda_3$, only major prolate regions were considered in this analysis. Prolate regions are defined as regions that contain eigenvalues with positive skewness [4]. Skewness is given by equation 1.9. Figure 2.2 shows the prolate regions that were considered for the analysis.

Another metric used for validation was using tensor overlap index (OVL) [12]. The OVL is defined by equation (2.10). The OVL is 0 when there is no overlap and

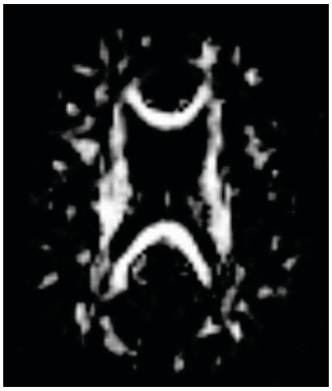

Figure 2.2: Prolate regions computed from the skewness value > 0.

is 1 for complete overlap between the three principal axes of the diffusion tensors. The average OVL of the voxels only in the prolate regions was considered after 0.2 FA thresholding was performed.

$$OVL = \frac{\sum_{i=1}^{3} \lambda_i \lambda_i (e_i . e_i)^2}{\sum_{i=1}^{3} \lambda_i \lambda_i} \tag{2.10}$$

Third type of quantitative analysis was an FA comparison. An overall average FA value was computed from both the reorientation techniques and compared with the reference FA map. We also checked the mean FA in the highly anisotropic corpus callosum. The corpus callosum was segmented manually from the original FA image using BRAINS2 [58].Figure 2.3 shows the segmented corpus callosum. This segmented region of interest (ROI) was used as a mask for computing the average FA for both the reorientation strategies.

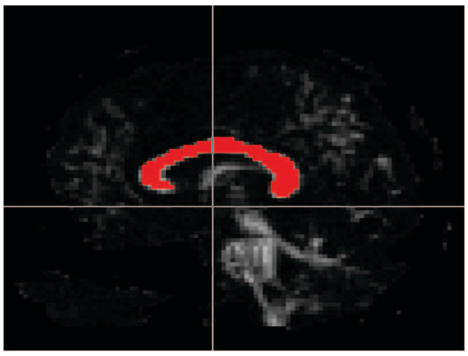

Figure 2.3: Segmentation of Corpus Callosum using BRAINS2.

2.1.2 Scan Rescan Reliability Testing

To determine the degree that noise was influencing the angular measurements, a scan rescan study was also performed. Three healthy subjects underwent a diffusion tensor imaging study after informed consent was obtained in accordance with the Institutional Review Board at the University of Iowa. The DWI scanning protocol described in the section 2.1.1 was used. Two repetitions of the DTI sequence were obtained within a single imaging session. During this study, the subjects head was kept in the same position for both diffusion tensor image acquisitions. The preprocessing of the diffusion data was performed using GTRACT software as described previously. The only difference was that each diffusion weighted image was aligned with the b=0 image from the first acquisition using a 12 parameter affine transform. The tensor image was then computed from registered diffusion data for both the visits. The angular dispersion and the OVL were computed between the tensors from acquisition 1 and 2.

2.1.3 Intersubject Non-linear Registration

For the evaluation of the gradient rotation method applied to nonlinear intersubject registration, the same data described in section 2.1.1 was used. One of the five subjects was chosen as the template or reference subject and the remaining four subjects were spatially normalized to the template subject. The preprocessing of DTI data was performed as described in the previous section. For the T1 anatomical datasets, an automated brain extraction was performed using AFNI 3dskullstrip (http://afni.nimh.nih.gov/afni) followed by a manual cleanup using BRAINS2 [58]. The anatomical dataset was used in the subsequent image registration steps.

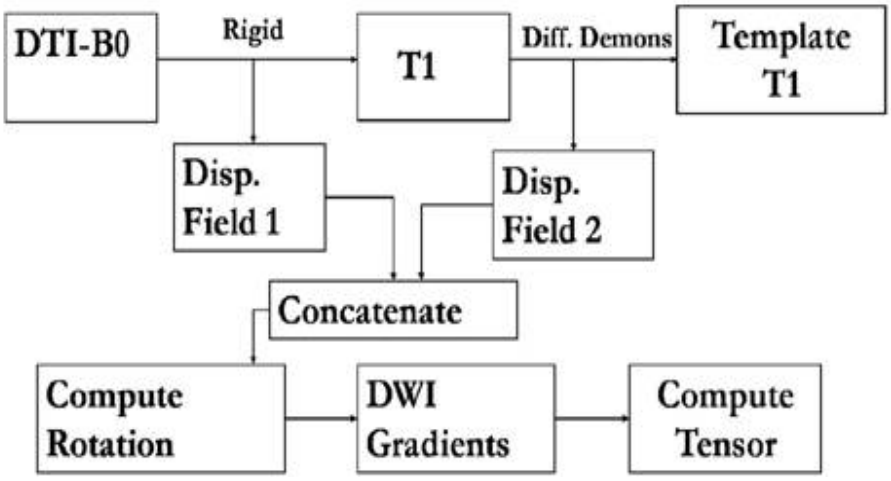

Figure 2.4: A multistage scheme for spatial normalization of tensors.

The idea of gradient rotation can be extended to a multi-stage registration sequence. The DTI b=0 image was co-registered to the anatomical T1-weighted image

for the corresponding subject using a rigid body transformation. Mutual information metric was used and the registration was initialized using the center of mass from the fixed and moving images. Figure 2.1.3 shows a flow chart for spatial normalization of the tensors. To account for intersubject heterogeneity in the brain, it is necessary to use a high order transformation to achieve alignment across subjects. Therefore, a diffeomorphic demons registration [84] was used to align subject T1 data and the template T1 image. This registration was initialized using a 12 parameter affine transformation. Similar to the rigid registration, the affine registration was initialized from the center of mass. A mutual information metric was utilized and the cost function of registration was minimized using gradient descent. The diffeomorphic demons method is based on Thirion Demons Algorithm [80]. The Thirion demons algorithm optimizes the displacement field space while the diffeomorphic demons algorithm optimizes the space of diffeomorphic transformations (i.e. maps one differentiable manifold to another, such that both the function and its inverse are smooth) [84]. A mean squared error metric was utilized and geometric optimization performed on a Lie group. The diffeomorphic registration was initialized using histogram matching between the moving and fixed image. A hierarchical registration was used with 3 levels of refinement (32x32x32, 64x64x64, 128x128x128) corresponding to 8mm, 4mm, and 2mm isotropic resolution. The affine registration was converted to a deformation field and used as the initial condition for the diffeomorphic demons registration.

Two separate displacement fields were computed from the resulting transformation, one from the rigid body registration and the second from the diffeomorphic

demons registration. These displacement fields were concatenated such that the size and spacing was equal to the template image. A rotation matrix (R) at each voxel was calculated from the displacement field using equations (2.1) and (2.2). The Jacobian was computed from the neighboring voxel displacements. The gradient vector at each voxel was corrected by using equation (4). The diffusion tensor field was then estimated using a least squares fitting method with background thresholding at an intensity value of 80 on the b = 0 image.

The quality of registration was evaluated by computing the Jaccard ratio (also known as Tannimoto coefficient) between each subject and the template. Jaccard is a ratio of intersection volume and union volume of the fixed image and the warped moving image [64]. The Jaccard was calculated using BRAINS2 for both the affine and diffeomorphic demons registrations. To access the quality of registration on the underlying white matter architecture, the angle in each voxel, between the PD of the template tensor image and PD in the transformed image was computed using equation (2.9) and the OVL between the PD's was computed using equation (2.10). The resulting angle signifies the relative orientation between the reoriented and reference image. A comparison was performed between the angles from initial affine transformation and after performing the diffeomorphic demons registration. The areas containing only prolate tensors, based on skewness value, were considered.

Four tensor rotation methods (tensor rotation, gradient rotation, tensor PPD and gradient rotation using PPD) were compared using the multistage registration scheme. For the gradient rotation methods, the scheme shown in figure 2.1.3 was

used while for tensor reorientation the rotation was applied to the tensors directly. The comparison of the four methods was performed by computing the angle and OVL between the reference tensor and the reoriented tensor as described in section 2.1.1.

2.1.4 Gradient rotation applied to Q-ball imaging

Preliminary test was performed on Q-ball numerical phantom data and human data. The numerical phantom was created with orthogonally crossing fibers, using a b value of 20000 and 64 vertices of a regularly tessalated hemisphere. Figure 2.1.4 shows the numerical phantom overlaid on a FA map. A 45 degree rotation was applied to the underlying FA map. The displacement field based on the rigid body registration was used for rotating the gradients. Another test on the numerical phantom was carried out by applying a landmark based non-linear displacement field as shown is figure 2.1.4.

A healthy subject underwent a DTI imaging after informed consent was obtained in accordance with the Institutional Review Board at the University of Iowa. The data was acquired on a 3T Siemens TIM Trio scanner using a 12 channel head coil. The parameters used were TR/TE =4700/114 msec, FOV=220x220 mm, matrix=128x128, voxel size=1.7/1.7/4 mm, 30 slices, 64 diffusion gradient orientations (0 and 3,000 s/mm^2) with 3 averages. The DTI data was co-registered using diffeomorphic demons registration with a template FA image [42]. The diffusion weighted signal vector was parameterized with spherical harmonic (SH) series (l_{max}=6) and odd harmonic orders were eliminated. QBI reconstruction was performed using the regularized analytic Funk-Radon transformation [82].

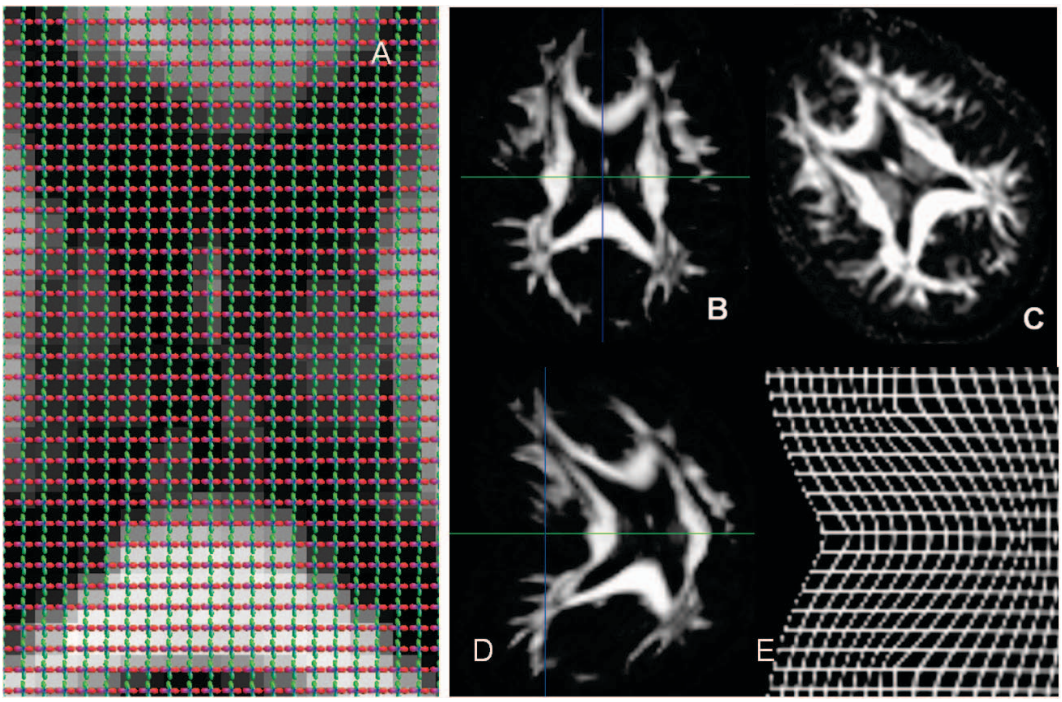

Figure 2.5: Q-Ball Numerical phantom (A) Crossing fibers phantom (B) Original FA (C) Rotated FA map (D) Deformed FA using non-linear deformation field (E) Non-linear deformation field

2.2 Multichannel Diffeomorphic Registration

The diffeomorphic demons algorithm proposed by Vercauteran [84] is an extension of Thirion demons algorithm [80]. The demons algorithm is based on optical flow equation. In the demons algorithm, when registering a moving volume M with a fixed volume F an update vector field u is computed at every iteration by minimizing the error E with respect to u as given in equation 2.11. A closed form solution of this minimization is given by equation 2.12. J is the gradient vector and σ_x is dependent upon the maximum step length. The displacement field is regularized using a gaussian kernel. The updated displacement field is computed either by using additive method s $\leftarrow$ s+u or by using compositive method s $\leftarrow$ s $\circ$ (Id+u).

$$E(u) = ||F - M \circ (s+u)||^2 + \frac{{\sigma_i}^2}{{\sigma_x}^2} * ||u||^2 \tag{2.11}$$

$$u = -\frac{F - M \circ s}{||J||^2 + \frac{{\sigma_i}^2}{{\sigma_x}^2}} J^T \tag{2.12}$$

The non-parametric diffeomorphic demons algorithm adapts the optimization procedure to the space of diffeomorphic transformations. This is done by implementing an intrinsic update step s $\leftarrow$ s $\circ$ exp(u). Constraining the transformation to be diffeomorphic facilitates to preserve the topology and prevents folding [84]. Also, diffeomorphic functions are bijective such that the inverse transformation is always smooth.

We have extended the diffeomorphic demons registration to include multiple

channels. Guimond et al proposed a multichannel extension for demons algorithm that included only rotationally invariant indices. The update field for each channel was computed seperately and then averaged. In our proposition, the coupling between the channels is based on FA value. When computing the gradient and the speed value, if the FA value is lower than the defined threshold, only the anatomical data is considered while in the white matter regions, tensor components are given more significance. The equation from Guimond et al [35]can be transformed to equation 2.13, where w indicate the weights defined for each channel based on FA thresholding. In each iteration, when the moving image is warped, the tensors can be reoriented using finite strain method introduced by Alexander [4].

$$u = -\frac{1}{\sum_{c=1}^{n} w_c} \sum_{c=1}^{n} w_c \frac{F_c - M_c \circ s}{||J_c||^2 + \frac{{\sigma_{ci}}^2}{{\sigma_x}^2}} * J_c \tag{2.13}$$

To evaluate the registration between each subject and the template, the relative angle and the OVL was measured. The angle measurement and the OVL are described in section 2.1.1.

2.2.1 Validation of Multichannel Registration

5 healthy subjects were used for the validation. The scanning protocol was as described previously in section 2.1.1. Diffusion weighted images and T1-weighted images were acquired. The preprocessing on these images was performed as described in section 2.1.1. One of the subjects was chosen as the template subject.

A multistage registration scheme was used for spatial normalization as shown

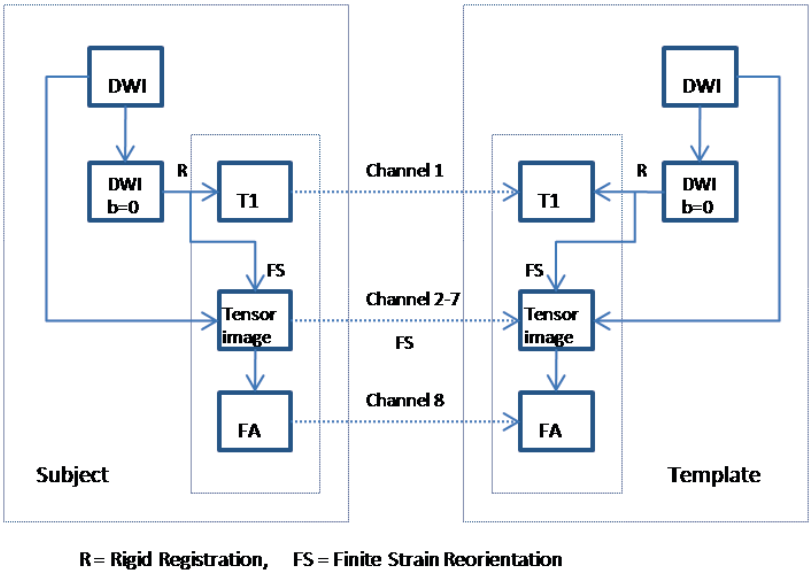

Figure 2.6: A scheme for spatial normalization of tensors using multiple channels

in figure 2.2.1. In the first step of the multistage registration, DTI non-weighted (b=0) image was co-registered to the anatomical T1-weighted image for the corresponding subject using a rigid body transformation. A mutual information metric was used and the registration was initialized using the center of mass from the fixed and moving images. The rigid body transform was applied to the tensor volume. The tensors were reoriented using the rotation matrix from the rigid body transform and the FA volume was computed.

In the second step, the intersubject registration was carried out using multi-channel diffeomorphic demons algorithm. This registration was initialized using a 12 parameter affine transformation between the T1-weighted volume of the subject and T1-weighted template volume. Similar to the rigid registration, the affine registra-

tion was initialized from the center of mass. Mutual information metric was utilized and cost function of registration was minimized using gradient descent optimization method. For the multichannel diffeomorphic demons registration, a vector image consisting of 8 channels i.e. T1-weighted, FA and six tensor elements was formed. While forming the vector image, the T1-weighted images were normalized and a histogram matching procedure was performed. A mean squared error metric was utilized and geometric optimization performed on a Lie group by computing the update field exponential. The maximum step length was defined to be 1.0 and the gradient computation was based on symmetrization of the demons forces. Registration was carried out between 7 channels i.e. T1-weighted and 6 tensor components, while the eighth channel (FA) was only used for defining the connection between the channels. For the regions where FA was lower than 0.2, 100 percent registration was driven by T1- weighted data, while when FA was greater than 0.2, 40 percent registration was based on T1-weighted and 10 percent weight was given to each tensor component. The tensors were reoriented using the finite strain strategy at each iteration.

To evaluate the registration between each subject and the template, the relative angle and the OVL was measured. The angle measurement and the OVL are described in section 2.1.1.

For a comparative study, we used single channel diffeomorphic demons registration between the T1-weighted images as described in section 2.1.4. We applied the final deformation field to the tensors and then reoriented the tensors using finite strain method. In the second case, we used a dual channel diffeomorphic demons

registration consisting of T1-weighted and FA information. For areas with FA lower than 0.2, T1-weighted volume was used while for areas with FA greater than 0.2, T1 and FA were weighed equally. The framework is generalized such that any number of channels can be used and the weights can be specified.

2.3 Group Analysis

Diffusion tensor imaging (DTI) has been used to study white matter in more detail. The purpose of this study was to evaluate gross white matter changes in schizophrenia using DTI.

Two separate studies were performed using different populations. In the first study, the analysis was based on FA values while in the second study the analysis was based on the whole diffusion tensor.

2.3.1 Study using FA analysis

Before developing the novel spatial normalization technique described in section 2.1.3, a pilot population study was performed using FA as the response variable. Instead of performing the non-linear intersubject registration, the analysis was based on coarse Talairach based parcellation of the white matter within the cerebral lobes (frontal, temporal, parietal, occipital and subcortical) as shown in figure 2.3.1. Subsequently a finer analysis using 1232 of the Talairach boxes was performed [78]. The Talairach atlas is shown in 2.3.1.

For this study, 17 male patients (mean age 28.5) with schizophrenia and 21 male control subjects (mean age 29.9) were recruited into an imaging study. The

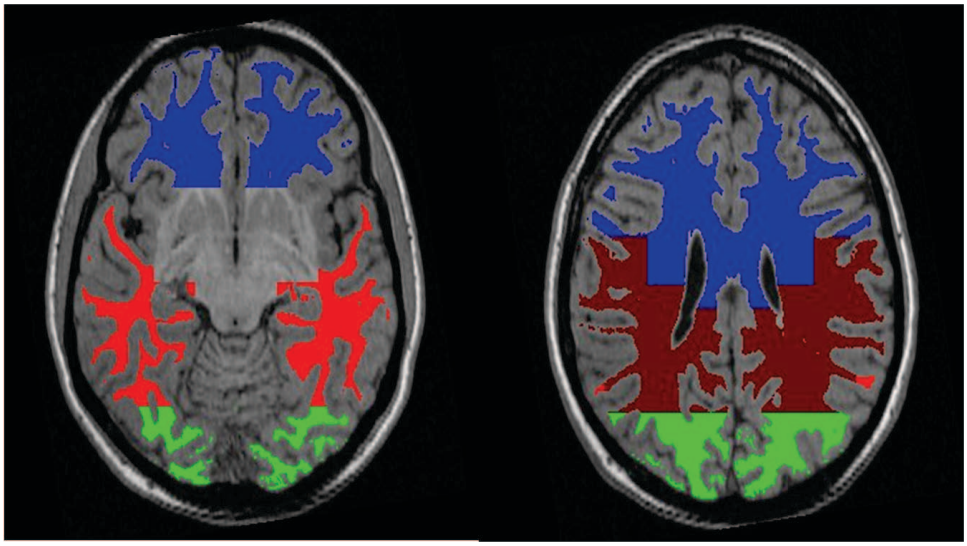

Figure 2.7: T1 weighted image with overlaid white matter masks for the frontal (blue), temporal (red), parietal (dark red) and occipital lobes (green) used to measure FA values.

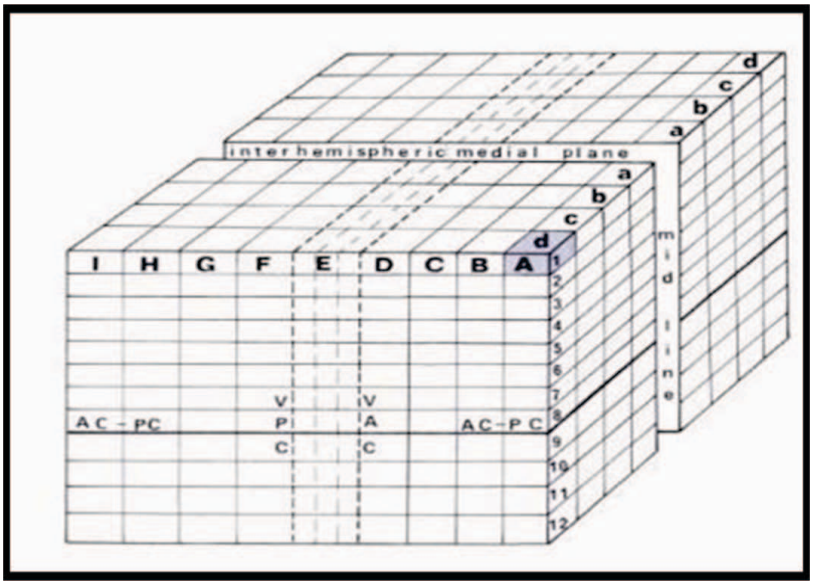

Figure 2.8: Figure showing all the Talairach boxes

subjects underwent a multi-modality imaging study to obtain anatomical T1 and T2 images using a 1.5 T scanner. DTI data was acquired on a 3T Siemens Trio scanner using six directions of diffusion encoding and a b-value of 1000. The anatomical images were processed using a standard image analysis pipeline including AC-PC alignment, tissue classification, and automated extraction of the brain using the BRAINS [58] software. The DTI images were analyzed using the GTRACT [23] software in a standard manner that included motion and eddy current correction, spatial filtering with a median filter, generation of diffusion tensor, and generation of fractional anisotropy (FA) images. The DTI data was co-registered with the AC-PC aligned T1 weighted images using a rigid registration and a mutual information registration metric. This was used as an initialization for a non-linear B-spline registration to correct for susceptibility distortion in the images. After the images were non-linearly aligned, a lobar Talairach based parcellation of cerebral white matter was performed and the average anisotropy was measured within these regions (figure 2.3.1). The white matter was defined based on the tissue classified image and limited to the cerebrum.

Ttests were carried out between the controls and patients while controlling for age. The null hypothesis was that the fractional anisotropy (FA) values in both the groups was equal. The second type of analysis was performed by measuring the mean FA values in each coronal slice from anterior to posterior part of the brain as shown in figure 2.3.1. T-tests were performed between patient and control groups.

Finally, for comparison, a more refined analysis of the FA images was conducted using SPM5 and TBSS tool from FSL [75]. In SPM5 anatomical images were

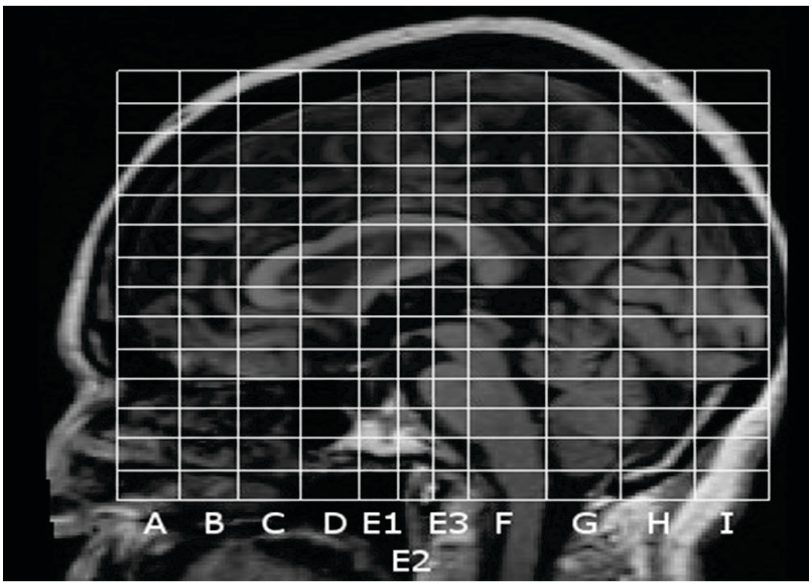

Figure 2.9: The coronal slices from A to I that were used for anterior to posterior FA analysis.

co-registered to the MNI 152 subject average brain. The anatomical images were coregistered using the discrete cosine nonlinear algorithm. The resulting transform was applied to the FA images. A two group t-test was performed on a voxel by voxel basis. While in FSL, non-linear registration was performed to align the FA data into a common space. The mean FA image is then created and thinned to create a mean FA skeleton which represents the centers of all tracts common to the group. Each subject's aligned FA data is then projected onto this skeleton and the resulting data is fed into voxelwise cross-subject statistics [75].

2.3.2 Study using tensor analysis

For this study, 9 patients (mean age 31.1) with schizophrenia and 9 control subjects (mean age 27.42) were recruited into an imaging study. The subjects underwent a multi-modality imaging study to obtain anatomical T1 and T2 images using a 1.5 T scanner. DTI data was acquired using thirty directions of diffusion encoding and a b-value of 1000. One of the subjects was chosen as the template subject. The anatomical images were processed using a standard image analysis pipeline including AC-PC alignment, tissue classification, and automated extraction of the brain using the BRAINS [58] software.

The DICOM diffusion-weighted image data were first converted into nrrd format(http://teem.sourceforge.net/nrrd/index.html). During this process, the Siemens mosaic images were unpacked and the gradient directions converted into the subject frame of reference. The diffusion weighted images were then corrected for motion and eddy current artifacts using the GTRACT software'[23]. To achieve this, the b=0 image served as a reference image and all other diffusion weighted images were matched using a mutual information metric [87] and subsequently aligned by an affine transformation. These motion correction parameters were also used to adjust the diffusion sensitizing gradient orientation.

For the spatial normalization of tensor images, the scheme as described in section 2.2.1 was implemented. In the first stage an intrasubject rigid registration was performed while in the second stage a multichannel diffeomorphic demons registration was performed. The multichannel registration was implemented using 8 channels

(T1- weighted, FA and 6 tensor components). All the channels were weighted equally when FA > 0.2 otherwise only T1-weighted image was considered. The registration was carried out using 3 levels of refinement. In the first two resolution levels, only the T1-weighted image was considered. In the last resolution level all eight channels were considered. This procedure decreases the time required for registration and also the tensors are not averaged at lower resolutions.

2.3.2.1 Tensor Analysis

Due to the recent development of the novel log-euclidean metric proposed by Arsigny et al., diffusion tensors can be transformed from the nonlinear space to their matrix logarithms in a euclidean space [8]. As in the scalar case, the matrix logarithm is defined as the inverse of the exponential. The uniqueness and the existence of the logarithm is not guaranteed for an invertible matrix. But the logarithm of a tensor is well-defined and is a symmetric matrix. Conversely, the exponential of any symmetric matrix yields a tensor. This means that under the matrix exponentiation operation, there is a one-to-one correspondence between symmetric matrices and tensors [8]. Based on this property, a vector based structure on the tensors can be defined.

The logarithm of a tensor can be computed by decomposing the tensor into its eigenvalues and eigenvectors. Taking the natural logarithm of the eigenvalues and then composing the eigenvectors and the diagonal eigenvalue matrix gives the logarithm of the original tensor. Based on this easy computation, tensor interpolation, averaging etc can be defined. Equation 2.14 shows the logarithmic multiplication

between two tensors S_1 and S_2 defined by $\odot$.

$$S_1 \odot S_2 = exp(log(S_1) + log(S_2)) \tag{2.14}$$

A simple similarity invariant log-euclidean metric is given by equation 2.15. Contrary to the affine-invariant case [30], the processing of tensors in the Log-Euclidean framework is simply Euclidean in the logarithmic domain.

$$dist(S_1, S_2) = Trace((log(S_1) + log(S_2))^2)^{\frac{1}{2}} \tag{2.15}$$

For simplifying the computations, the tensor matrix can be considered as a 6-D vector and the logarithm can be computed as shown in equation 2.16.

$$log(S) = [log(S)_{1,1}, log(S)_{2,2}, log(S)_{3,3}, \sqrt{2}.log(S)_{1,2}, \sqrt{2}.log(S)_{1,3}, \sqrt{2}.log(S)_{2,3}]^T \tag{2.16}$$

For the group analysis of diffusion tensors, a linear regression model with the log transformed diffusion tensors as responses, is used [55]. If n number of subjects are used in the analysis, we get n tensors from the corresponding voxel of the spatially normalized data. If we compute the logarithm of each tensor by using equation 2.16, a linear model for such a tensor S_i, $i = 1, .. n$, is given by Equation 2.17.

$$log(S_i) = \beta x_i + \epsilon_i \tag{2.17}$$

where,

$$\beta^T = [\beta_1, ...\beta_6] \tag{2.18}$$

is a px6 matrix representing the regression coefficients. ϵ_i is the error given by,

$$\epsilon_i = [\epsilon^i_{(1,1)}, \epsilon^i_{(2,2)}, \epsilon^i_{(3,3)}, \epsilon^i_{(1,2)}, \epsilon^i_{(1,3)}, \epsilon^i_{(2,3)}]^T \tag{2.19}$$

x_i is a px1 vector that contains clinical variables like age, gender etc. An simple linear regression model is as given in equation 2.20. If two groups are compared, then we can set x_i such that 1 corresponds to the intercept and δ in an indicator of one of the groups.

$$log(S_i) = \begin{pmatrix} \beta_{1,1} & \beta_{1,2} \\ : & : \\ \beta_{6,1} & \beta_{6,2} \end{pmatrix} \begin{pmatrix} 1 \\ \delta \end{pmatrix} + \epsilon_i \tag{2.20}$$

A hypothesis testing was carried out to understand the differences between the controls and patients. Based on the method proposed by Li et al., the linear hypothesis was given as shown in equation 2.21 [55].

$$H_0 : R\beta = b_0 \quad vs. \quad H_1 : R\beta \neq b_0 \tag{2.21}$$

where β is a 6p x 1 vector, R is an rx6p matrix of full row rank and b_0 is an r x 1 specified vector [55]. Details for computing the test score statistics can be found in [55], [54].

The tensor analysis was performed on the spatially normalized tensors described in section 2.3. All the tensor images were masked using a binary mask computed from the template T1-weighted volume.

Full diffusion tensors were treated as response and the model given in equation 2.20 was chosen. The δ value for controls was 0 while for patients with Schizophrenia it was 1. Here R was 6x12 matrix while $b_0 = (0,0,0,0,0,0)^T$ for the hypothesis. The uncorrected p-values < 0.01 were mapped on the MNI- template brain and then clustered using afni (http://afni.nimh.nih.gov/afni).

We compared the tensor results using an equivalent FA study. The FA images of all the controls and patients used in tensor analysis, were used in voxel-wise group analysis performed using FSL software [75]. This was done to verify the results given by the log-euclidean tensor analysis.

Another comparison was performed using the Geodesic Anisotropy (GA) index. The geodesic anisotropy measure is derived from the tensor manifold metric. The GA that is implemented in our analysis, was computed using the log-euclidean metric [51]. GA index was used an alternative scalar measure to compare the results from the tensor analysis and the FA analysis. Equation 2.22 defines the GA of a tensor. The GA value can be normalized by computing its hyperbolic tangent value as given in equation 2.24 [13]. A voxel-wise t-test was performed between the controls and the patients based on GA values. A false positive correction was performed by using false discovery rates (FDR) method. The areas where q-value < 0.05 were clustered and mapped in the MNI space using afni (http://afni.nimh.nih.gov/afni).

$$GA(S) = \sqrt{(Trace(log(S) - < log(S) > I)^2)} \tag{2.22}$$

where,

$$< log(S) >= \frac{Trace(log(S))}{3} \tag{2.23}$$

$$tGA = tanh(GA) \tag{2.24}$$

2.4 Data Sharing

The complete framework that includes multichannel registration and gradient rotation is an open source package written using ITK and is available from the Neuroimaging Informatics Tools and Resources Clearinghouse (NITRC) website, (http://www.nitrc.org/projects/diffusionwarp). This resource will be used to house all of the source code using the SVN features, distribution binary and source code releases, and documentation for the tool. The bug tracking and mailing list features from the NITRC website will be utilized to support the software development process and to announce new features and releases of the software. The software will be licensed using a BSD style license allowing commercial system to integrate this tool within their products.

CHAPTER 3
RESULTS

3.1 Gradient Rotation

3.1.1 Intra-subject Gradient Rotation Validation

Figure 2.1.1(C) shows the quality of registration used for the intra-subject gradient and tensor rotation methods. The reference image tensor representation of the DWI data from the first sequence (head in normal position) is shown in Figure 2.1.1(A). Qualitatively the two methods produce similar results and generate tensors that are similar to the reference data. Figure 3.1 shows the tensor representation of when gradient rotation is applied (3.1(B))and when tensor reorientation is applied (3.1(C)) compared to the reference (3.1(A)).

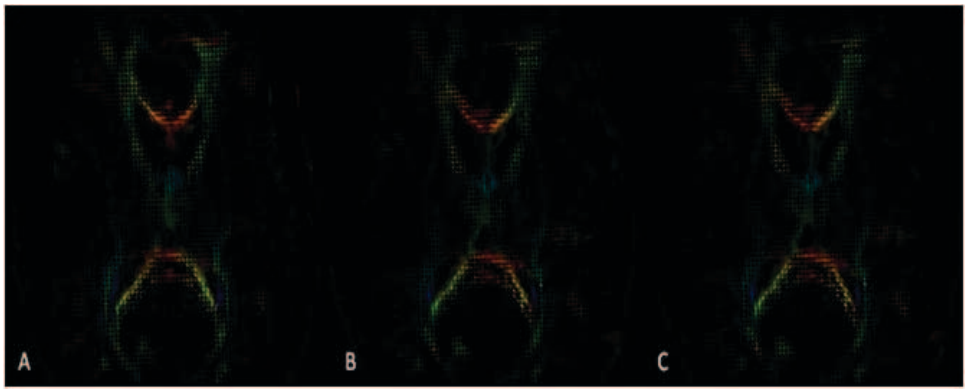

Figure 3.1: Tensor representation of A. Reference image B. After applying gradient rotation and C. After applying tensor reorientation

Figure 3.2 shows the tensor representation of the genu of corpus callosum for one of the subjects. Figure 3.2(A) illustrates the original tensor computed from the normal head position. The tensor was smoothed using a gaussian filter with σ =1. Figure 3.2(B) shows the image rotated when no tensor reorientation was applied. Figure 3.2(C) demonstrates the results from the gradient rotation method while figure 3.2(D) illustrates the tensor reorientation method.

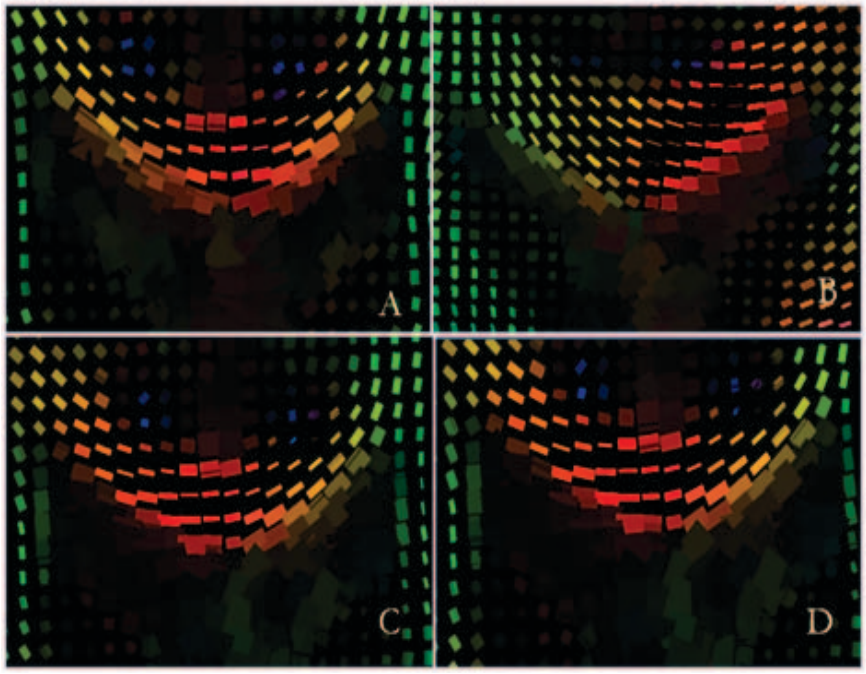

Figure 3.2: Axial tensor glyph maps of the genu of corpus callosum. (A) Original tensor from DWI dataset. (B) Without any reorientation applied. (C) Results from gradient rotation method and (D) tensor reorientation.

The average angular separation between the reoriented tensor and the reference tensor was computed for both the reorientation techniques. For the gradient

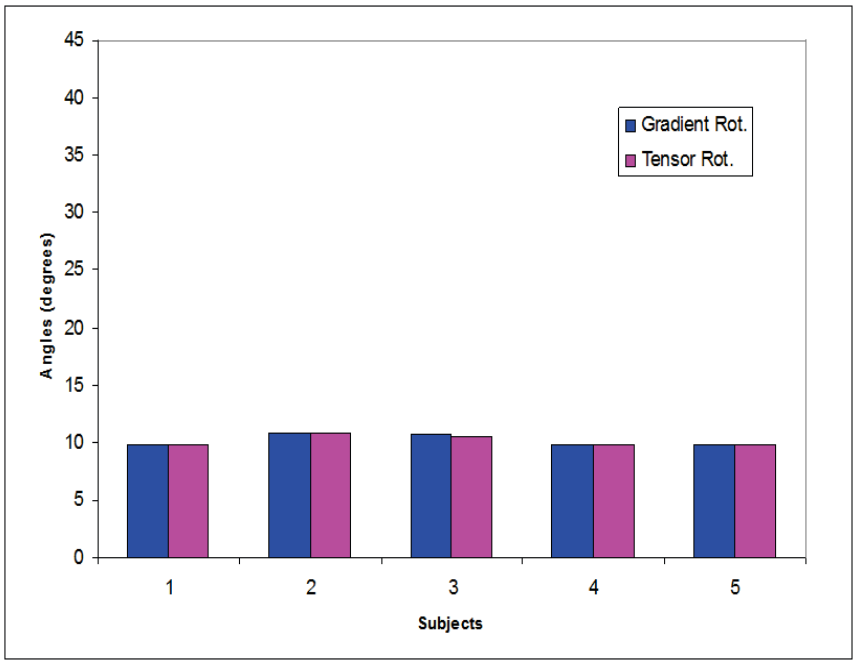

Figure 3.3: Plot of average angular deviation for each subject using the two comparative reorientation methods.

rotation method, the average value was 10.18° across all 5 subjects while for tensor reorientation the average value was 10.16°. Figure 3.3 shows the angular deviation for each subject using gradient rotation and tensor reorientation techniques. The average OVL for both the methods was 0.89.

Table 3.1: Average and Standard deviation in FA for all 5 subjects

-	Reference Tensor	Gradient Rotation	Tensor Reorientation
Average FA	0.359	0.34	0.345
Std. Dev	0.006	0.0065	0.007

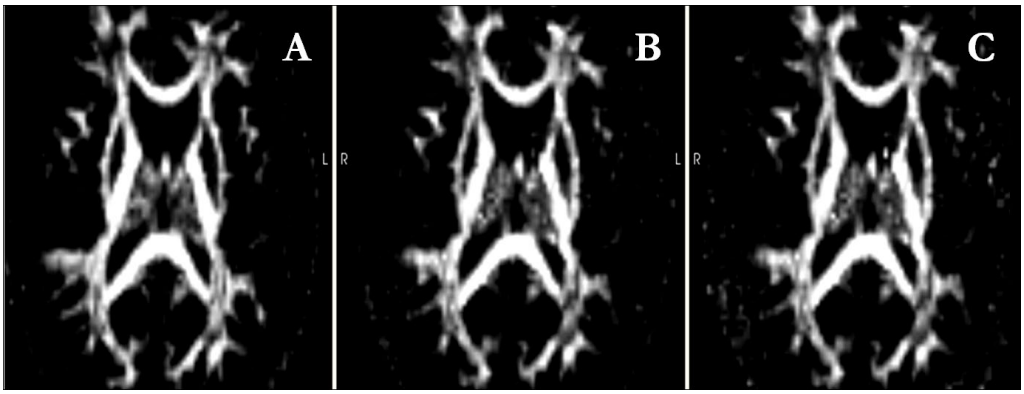

Figure 3.4: Comparison using FA maps of a subject (A) FA in normal head position (reference image) (B) FA after gradient rotation, and (C) FA after tensor reorientation.

The methods were also compared using the FA scalar measures. Figure 3.4 shows the FA maps of the original tensor and the two reorientation methods. Table 3.1 shows the average FA values. This indicates that the average FA values from the reorientation techniques are comparable to the original FA. No significant differences were found between the resulting FA values from gradient rotation and tensor reorientation ($p = 0.31$). Figure 3.5 shows the FA values in the corpus callosum for both reorientation methods compared with the reference image. The standard deviation for each case is indicated with error bars in the graph. Results indicate that the FA values after transformation are comparable with the reference image FA values in corpus callosum.

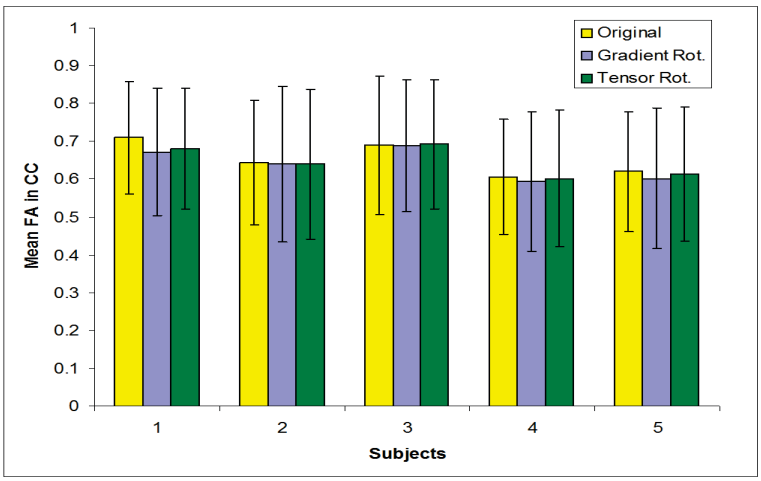

Figure 3.5: Plot of average FA in corpus callosum for 5 subjects. The 3 cases, i.e. reference, gradient rotation and tensor reorientation are shown. The error bars show the standard deviation of the FA values within the corpus callosum for each subject.

3.1.2 Scan-Rescan Reliability Testing

Figure 3.6(A, B) show the principal eigenvector image for one of the subjects scanned with separate acquisitions. The images reflect the results after registering with the b=0 image from the first acquisition. The average angle between any two visits for 3 subjects is 9.17° with an average OVL = 0.9 without using any type of reorientation technique.

3.1.3 Intersubject Registration with Gradient Rotation

Figure 3.7(A and B) show the resulting rigid registration between the diffusion weighted images and T1 weighted anatomical images. Figure 3.7(C and D) show the diffeomorphic registration between T1 image of a subject and the template image. The moving image resampled into the space of the fixed image is shown in 3.7(C) while

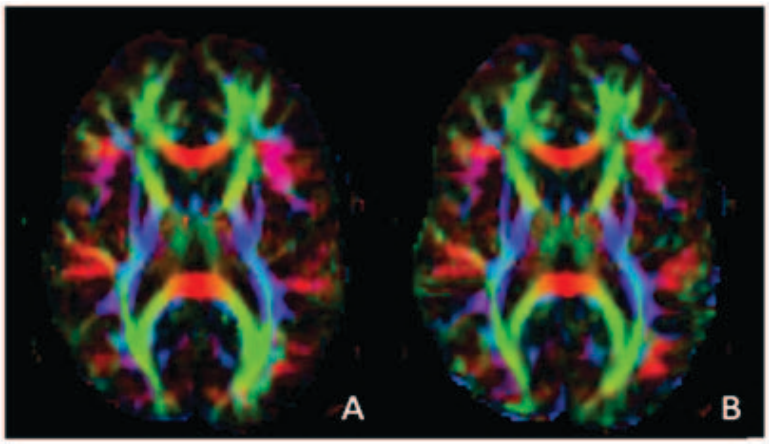

Figure 3.6: Results of scan-rescan reliability testing. (A, B): Principal eigenvector images after registration with T1 for visit 1 and visit 2 respectively for one of the subjects.

the template image is illustrated in 3.7(D). Figure 3.8 shows the principal eigenvector image of the gold standard reference image 3.8(A), and the principal eigenvector images of spatially normalized tensors for 4 subjects using gradient rotation in 3.8(B-E).

3.1.4 Comparison between all the reorientation methods

Qualitative results of the resulting tensor orientation for all four tensor rotation methods are a shown in an axial slice containing the genu and splenium of the corpus callosum (Figure 3.9). It can be observed that the tensors appear to be aligned consistently with the underlying white matter fiber orientation in all four cases. The results for the tensor overlap index and angular difference are shown in Figure 3.10(A). It can be observed that the tensor overlap is higher for the PPD

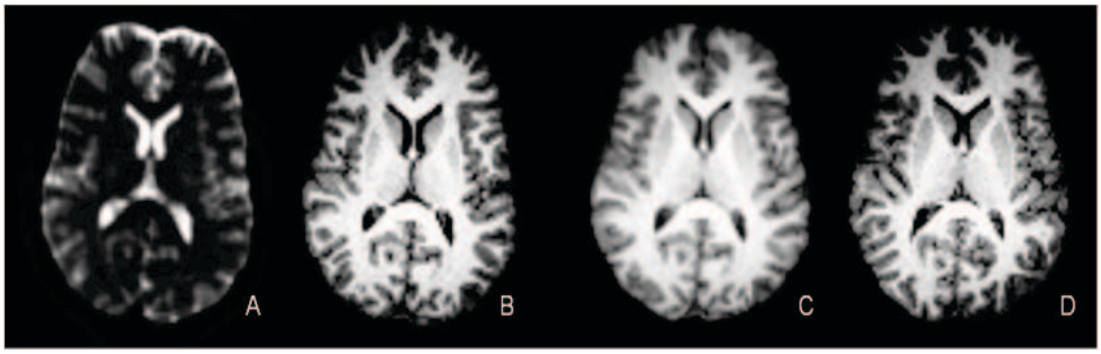

Figure 3.7: Quality of Registration (A) DTI b=0 resampled image after rigid registration (B) Fixed image (T1). (C) T1 resampled image after diffeomorphic demons registration. (D) Template or Reference T1 image.

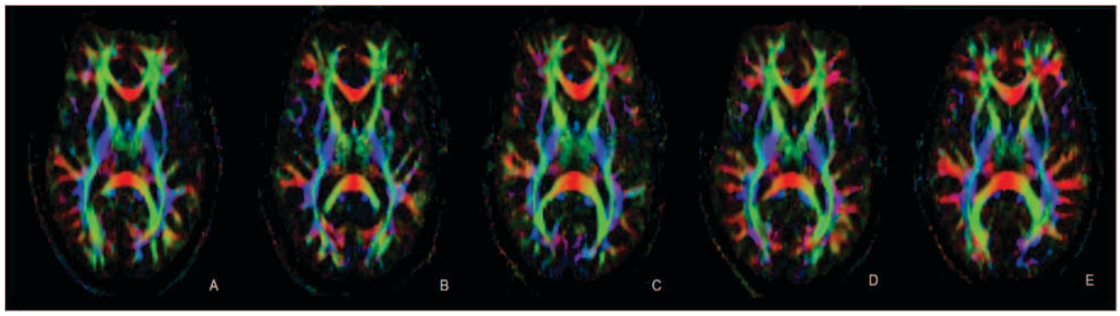

Figure 3.8: (A). Principal eigenvector image of the template (reference subject), and the four subject after registration with the template subject (B, C, D, E). Principal eigenvector images of the four spatially normalized subjects with respect to the reference image.

methods as compared to the rotation only methods. The average angular difference between the four subjects and the template image is plotted in Figure 3.10(B). The angular error after affine transformation is much higher compared to after nonlinear registration. The angle after diffeomorphic demons is approximately 21° (OVL = 0.76) for the rigid rotation methods (gradient rotation and tensor rotation) while it is approximately 19° (OVL =0.786) for both of the PPD methods.

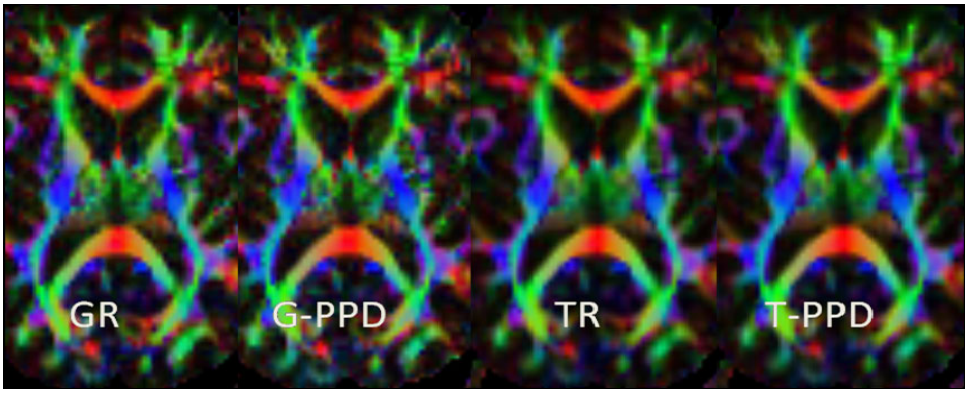

Figure 3.9: Primary eigenvector images color coded for the four reorientation methods from one of the subjects after the multistage registration for all the methods. (GR) Gradient Rotation, (G-PPD) Gradient rotation using PPD, (TR) Tensor rotation, (T-PPD) Tensor rotation using PPD

3.1.5 Gradient Rotation applied to Q-ball imaging

Figure 3.11 shows the results for the numerical phantom data. For the human data figure 3.12 shows the Q-ball reconstruction before and after gradient rotation.

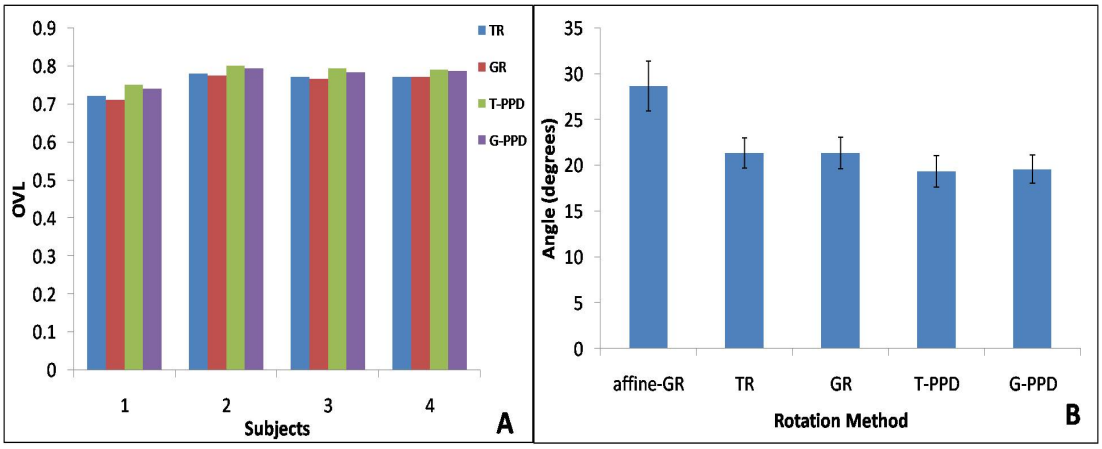

Figure 3.10: Plot of the overlap index (OVL) for four subjects as compared to the template image. Higher OVL values correspond to improved registration. Results are shown for the tensor rotation (TR), gradient rotation (GR), tensor PPD (T-PPD), and gradient rotation with PPD (G-PPD). (B). Plot of the average angular difference for the four methods. The first column shows the angular difference when only affine registration is used with gradient rotation. The other four columns show the results of using the diffeomorphic demons registration and each of the rotation methods.

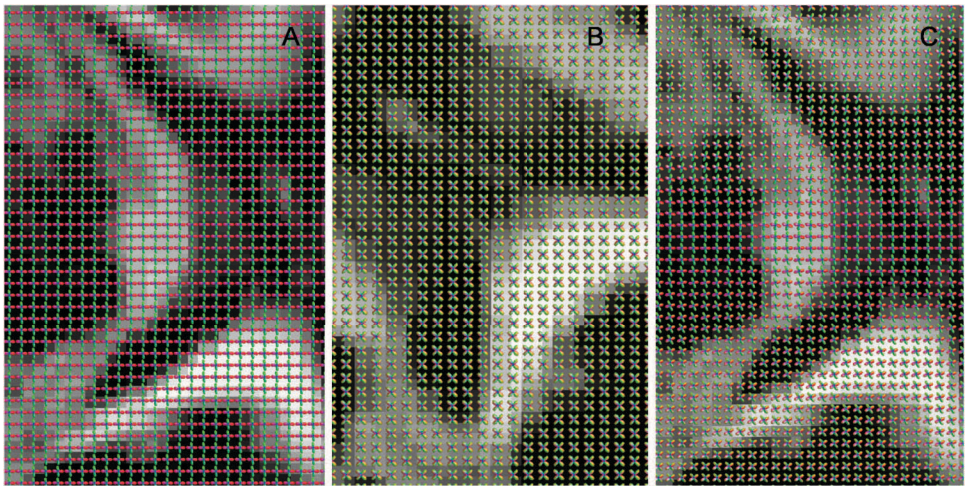

Figure 3.11: Results for q-ball model after using gradient rotation. (A) Original phantom (B) After rigid rotation (C) After nonlinear deformation

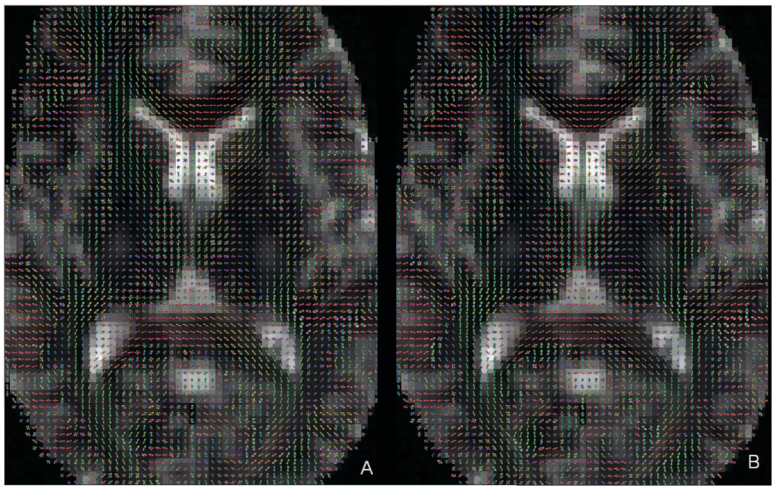

Figure 3.12: Results for q-ball model (A) Before (B) After gradient rotation

3.2 Multichannel Diffeomorphic Demons Registration

The tensor representation for one of the subject after registration is shown in figure 3.11. The single channel, dual channel and multichannel registration results are shown in figure 3.11(A, B, and C) respectively. Figure 3.11(D) is the fixed image. The average angle for four subjects using the single channel registration was 21°, for dual channel it was 20° and for multichannel registration the angle was reduced to 18.19°. Figure 3.12 shows the plot of average OVL for four subjects using the three comparative registration methods. It can be seen clearly, that the tensors overlap better when seven channels are used together. This can be shown by using a t-test between multichannel registration and the other two methods. The OVL values with multichannel registration were significantly greater than the single channel (p=0.0119). A similar trend was observed when compared to the dual channel

registration that involved T1-weighted data and FA together (p=0.087).

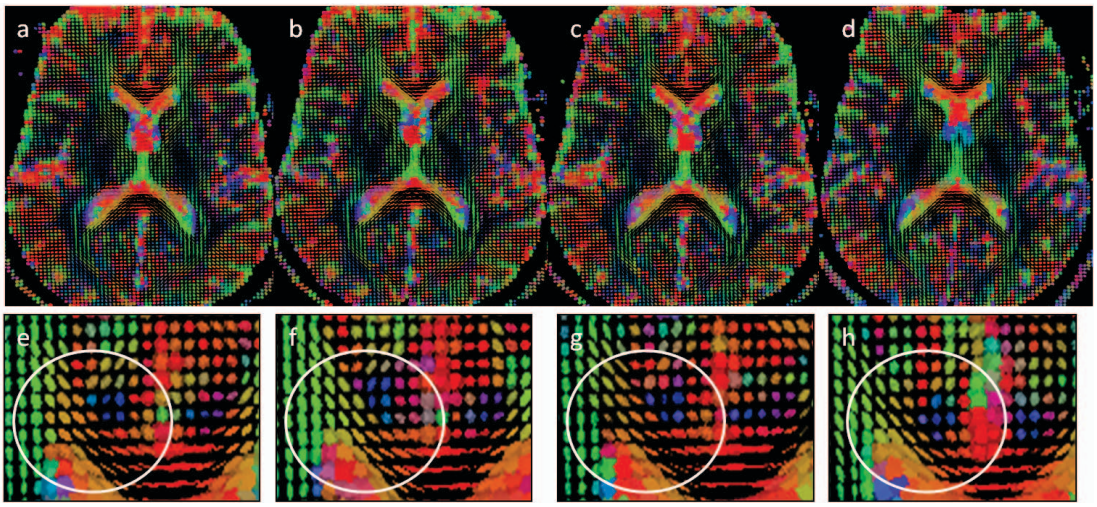

Figure 3.13: Registration results compared with the fixed image. (A) single channel result, (B)dual channel result, (C) multichannel result and (D) fixed image. (E,F,G,H) show the part of Genu from the four figures above. It can be observed that the results from multichannel registration closely match with the fixed image

3.3 Group Analysis of Controls and Patients with Schizophrenia

3.3.1 Pilot Analysis using FA

The results for the coarse Talairach lobar parcellation are shown in table 3.2.

After analyzing the 1232 Talairach boxes, significant changes in FA were observed in different parts of the brain. In the temporal and parietal lobe, reduction in FA was observed around the calcarine sulcus, right precuneus and the white matter bordering the insula. In the frontal lobe, although overall changes were not observed, the middle frontal gyrus and the left gyrus cingulate did show significant FA reduc-

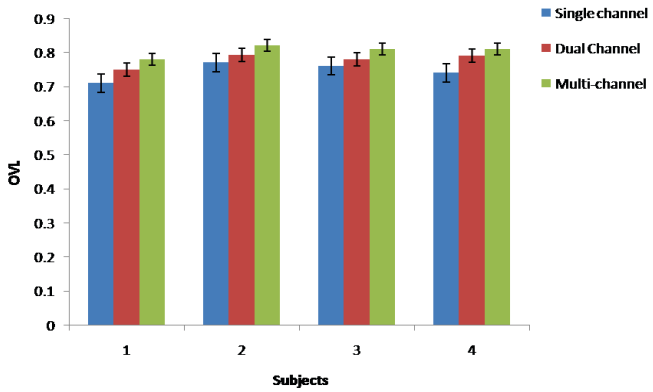

Figure 3.14: Plot of OVL for each subject using different types of registration.

Table 3.2: Table showing p-values for changes in FA in the brain lobes

Region	Left p-value	Right p-value
Frontal	0.965	0.431
temporal	0.072	0.034
parietal	0.021	0.014
occipital	0.158	0.189

tion.

Figure 3.15 shows the coronal sections from A to I that were considered for the anterior to posterior analysis. From the results it was observed that FA values reduced significantly in the parietal and temporal areas of the brain. These results match the lobar Talairach analysis since significant FA reduction was observed in the parietal and temporal lobes. Figure 3.15(A), (B) and (C) show the average anisotropy values in overall brain, right side and left side respectively.

The results after voxelwise FA analysis was performed using SPM are shown in figure 3.16. The regions that showed significant FA change included the anterior portion of the corona radiata and internal capsule (figure 3.16(A)) and also cerebellar vermis and inferior temporal lobe (figure 3.16(B)). There were no significant changes found in the FA values between the controls and patients using FSL, although differences are seen in the Talairach and SPM analysis.

3.3.2 Group Analysis using full diffusion tensors

Figure 3.17 shows the spatial normalization for 2 of the given subjects. Figure 3.17(A) is the reference subject. Figures 3.17(B) is a control and figure 3.17(C) is a patient. The quantitative analysis shows how well the subjects align with the template. Table 3.3 illustrates the average OVL and dispersion angle for each subject.

The results for the tensor analysis performed using linear regression on tensors in log-euclidean space as shown in figure 3.18. The significant raw p-values (below 0.01) were clustered and mapped on the MNI space using afni. Figure 3.18 shows the significant regions colored in orange. Figure 3.18(A) shows significant regions in

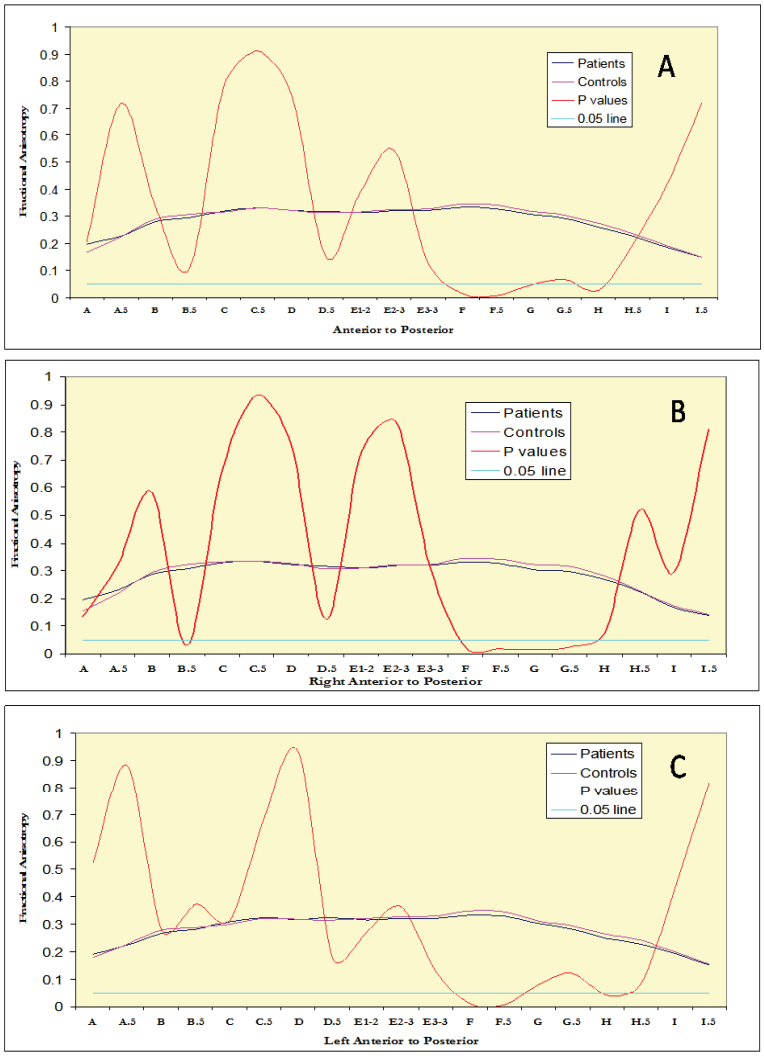

Figure 3.15: FA from anterior to posterior for controls (pink) and patients (blue). The p-values are indicated by red line. (A) Overall brain (B) Right side and (C) Left side

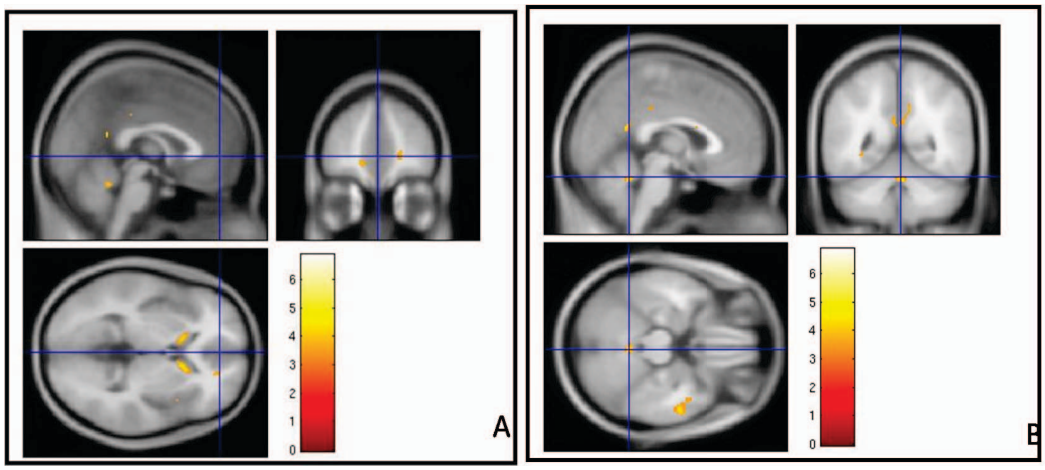

Figure 3.16: Results from SPM analysis showing the voxels with an uncorrected p value ≤ 0.001.

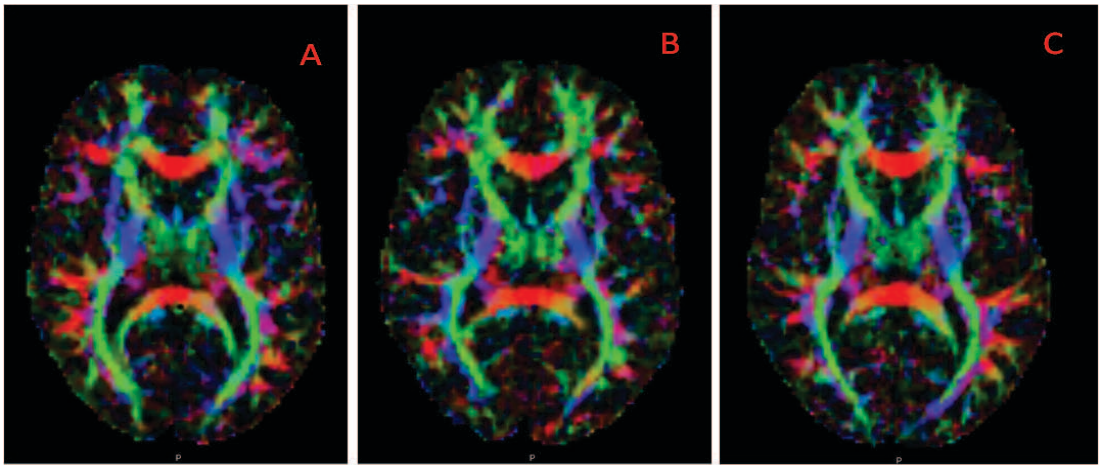

Figure 3.17: Figure shows the results of spatial normalization performed on controls and patients of Schizophrenia. The template image is shown in (A). As an illustration one of the controls is shown in (B) and one patient is shown in (C)

Table 3.3: Table showing the values of angular dispersion and tensor overlap index for 9 controls and 9 patients

Subject	Angle (°)	OVL
template	–	–
control 2	20.77	0.77
control 3	21.01	0.766
control 4	21.43	0.783
control 5	20.54	0.78
control 6	20.1	0.792
control 7	19.84	0.79
control 8	21.02	0.77
control 9	19.15	0.79
patient 1	21.63	0.77
patient 2	20.65	0.78
patient 3	21.24	0.777
patient 4	20.15	0.77
patient 5	20.77	0.76
patient 6	21.01	0.76
patient 7	22.18	0.746
patient 8	19.47	0.81
patient 9	20.01	0.787

Table 3.4: Table showing the mean and standard deviation of p-values in four clusters

Cluster	Mean	Std. Deviation
cluster 1	0.008	0.0012
cluster 2	0.0051	0.0013
cluster 3	0.0032	0.0011
cluster 4	0.0028	0.0013

the posterior corona radiata that relate to the primary motor cortex. Figure 3.18(B) shows some significant regions near the ventricles and the posterior end of corona radiata. In figure 3.18(C) white matter changes are specifically observed in the forceps minor (right), anterior limb of the internal capsule and posterior corona radiata. Figure 3.18(D) shows the significant areas that can be identified as part of genu of the corpus callosum and the forceps minor(left). A statistics on four of the major clusters is given in table 3.4. The mean and standard deviation of the p-values for each cluster were computed using afni.

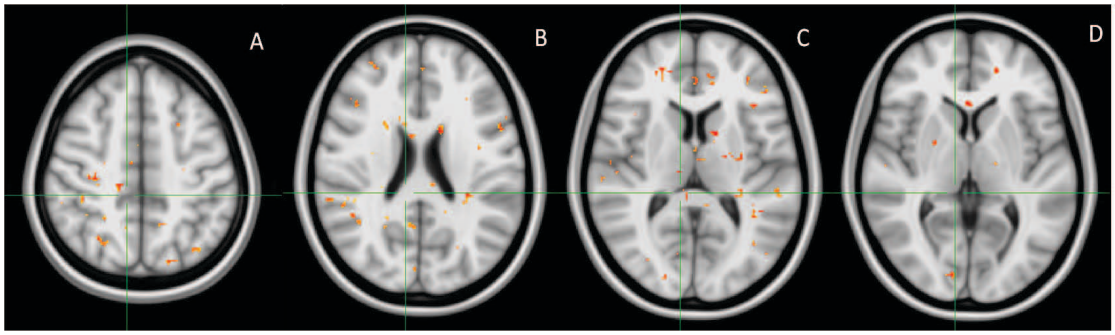

Figure 3.18: Clustered p-values below 0.01. The orange clusters show the significant regions that account for the changes in white matter anisotropy between the controls and patients after performing log-euclidean tensor analysis.

The results from the FA analysis using FSL are shown in figure 3.19. It can be observed that the FA reduces in patients in the areas colored red in figure 3.19. The areas can be identified as genu of the corpus callosum and the forceps minor. There were no areas where the FA in patients increased significantly.

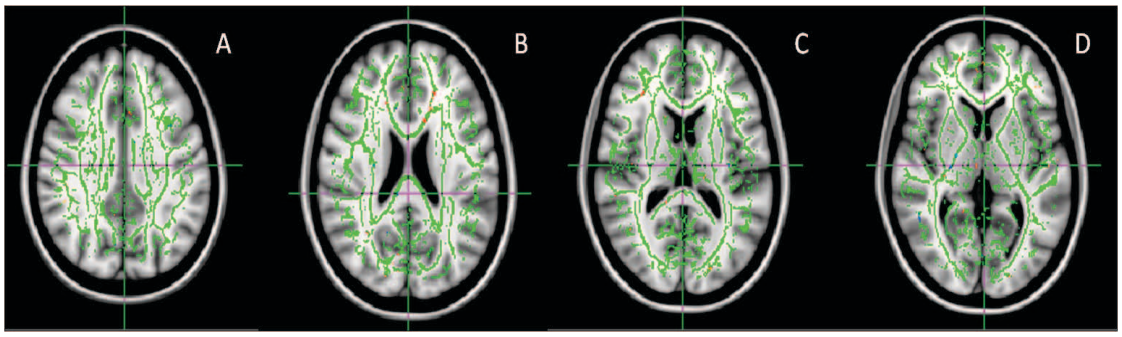

Figure 3.19: FA analysis using FSL. Red areas are the areas where FA is significantly lower in patients than controls.

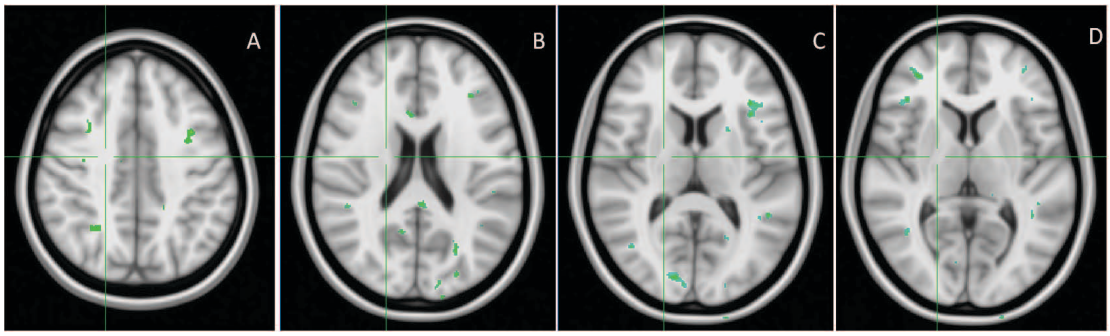

Figure 3.20: GA analysis performed between the spatially normalized controls and patients. Green areas signify the differences between the two groups.

The GA analysis results are shown in figure 3.20. The results from the t-test between the groups were corrected using false discovery rates. The significant areas with z-score higher than the threshold of 5 are shown in green in figure 3.20. In figure 3.20(A), the significant area can be identified as right posterior part of corona radiata. Other regions where a significant difference was observed are portions of genu and splenium of the corpus callosum as shown in figure 3.20(B), parts of anterior

corona radiata and forceps minor as shown in figure 3.20(C) and (D).

CHAPTER 4
DISCUSSION

In contrast to traditional MRI where the white matter appears homogeneous, diffusion imaging has the power to provide white matter architecture information. DTI takes advantage of the microscopic diffusion of water molecules, which is less restricted along the axis of a fiber than along its transverse direction. Tensor images are usually acquired by applying at least six non-collinear gradient orientations, and thus measuring a symmetric tensor in each voxel. The capability of diffusion tensor imaging can be implemented in studying effects of certain neurological disorders, development and aging.

The information contained in the diffusion tensors is very complex. Therefore a simple way of dealing with tensors is to compute rotationally invariant scalar quantities. Numerous population based studies have used scalar quantities like FA, RA, Volume ratio, Trace, eigenvalues etc. to discover the differences in the axonal architecture [45], [56], [7], [22], [73], [44], [10], [40].

By using scalar quantities for population based studies, the maximum power of diffusion tensor imaging may not be utilized in making scientific conclusions. Therefore a precise spatial normalization and interpretation focusing on the properties of diffusion tensors is required.

It is more complicated to apply spatial normalization to tensor fields than to scalar images. This is because the tensor must be reoriented on each image voxel, in

addition to a voxel displacement that is implied by the spatial normalization transformation [94].

In this thesis, a novel method for reorientation of tensors was proposed. In this method, rotations are applied to the diffusion sensitizing gradients providing a voxel-by-voxel estimate of the diffusion gradients instead of a volume of by volume estimate. The advantages of using the gradient rotation method are:

1. It can be applied directly to higher order models like q-ball model and high order tensors.

2. It eliminates the complex problem of tensor interpolation.

The rotation matrix computation is based on work by Alexander et al. [4]. Alexander, in his paper described two separate methods for computing the rotation matrix. One of the method was called as the finite strain method described in section 2.1. The other method was called as the preservation of principal direction (PPD) that included the shearing and stretching parameters in the rotation matrix computation. The algorithm for PPD is given in 2.1. The gradient rotation was build on both the reorientation techniques described by Alexander.

Validation of gradient rotation method was performed using a simple case of head rotation in the x-y plane. The gradients were rotated on a voxel by voxel basis, changing the b- matrix in each voxel, using an estimate of the rotation computed from the displacement field. For assessing gradient rotation method, relative orientations in the corresponding locations between the transformed tensors and the reference

tensor were observed. The method was also compared with Alexander's finite strain tensor reorientation method. The intrasubject average angular dispersion was around 10° for both the reorientation methods. Results are shown in section 3.1.1.

Looking at the intrasubject results, one may think that the average angular dispersion of 10° is very high. This is due to the low SNR of the diffusion images. To prove this a scan rescan reliability testing was performed using the same protocol as was used for the validation study described in section 3.1.1. All the gradient images from the second visit were aligned with the non-weighted image from the first visit. The average angular dispersion between the two visits was approximately 9°. If we go back in literature, a similar trend can be seen in the work performed by Alexander et al [4]. When the finite strain reorientation and the PPD reorientation was performed on numerical phantom data with no added noise, the resulting angular dispersion in the prolate regions was close to zero. But when a human dataset was used, the angular dispersion is between 8° to 11° for both the methods. Figure 4 shows the results from Alexander et al. Another study by Jones et al (2002) computed tensor dispersion plots, which showed a poor tensor overlap in the sub-cortical white matter regions [39].

A multistage registration scheme for the spatial normalization of tensors is proposed. The procedure is described in section 2.1.3. An example was illustrated using 5 subjects, one of them being the template subject. A simple rigid transform was used between the b=0 image and the T1 image while a nonlinear diffeomorphic demons registration was used for intersubject registration. The displacement fields

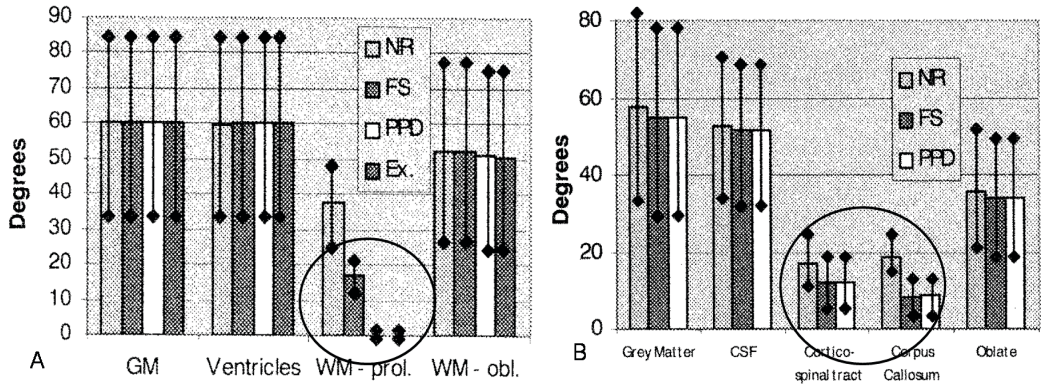

Figure 4.1: Comparative results from Alexander et al. (A) Numerical phantom (B) Human data

were concatenated from the two transforms and used for gradient rotation. The tensors were computed after gradient rotation was performed. Quantitative validation shows that the angle reduces after using diffeomorphic demons registration.

It has been shown by Alexander that the PPD method is more effective than rigid rotation since shear and scale are considered while using PPD. Gradient rotation can be extended to PPD using principal component analysis. We compared the existing methods of tensor rotation and PPD on tensors with the new gradient rotation and PPD with gradient rotation methods using the multistage registration scheme. The resulting angular separation was approximately 21° while it was slightly less - 19° for PPD methods since it accounts for shear and scale.

In recent years, more and more research groups are focusing high order diffusion models. This is because the tensor provides only a single fiber orientation estimate in each voxel and fails at fiber crossings. The gradient rotation method can

contribute in spatial normalization of these models.

While the overall global shape change has been minimized, there are still significant differences in the underlying white matter fiber architecture that need to be addressed. The registration method for tensors should be such that it can match the spatial location of white matter structures i.e. the fiber bundles correctly. Hence the registration should include the detection of anatomical correspondences as well.

Many tensor registration algorithms have been proposed upto this date [3], [95], [35], [65], [20], [97], [99], [53]. Many of these algorithms eliminate the complexity posed by tensor reorientation, by using scalar features. For example, Guimond et al., have used only scalar values like FA, trace etc. in the matching process. The output displacement field is applied to the tensors. They show that this orientation independent approach qualitatively compares in performance with an implementation of full tensor (plus T2-weighted intensity) registration with finite-strain reorientation and outperforms scalar registration using only the T2-weighted information [33]. Ziyan et al., have made use of fibers extracted through tractography [99] while Leemans et al. match the diffusion weighted images and then compute the tensor [53]. Some methods register actual tensor images, but do not reorient the tensor during registration [71].

Alexander and Gee [3] introduced an elastic matching algorithm based on tensor similarity measures. Reorientation was performed using the preservation of principal direction (PPD) method after each iteration. The similarity measures allow structural data to be considered with the tensor information by averaging the

similarities from two modalities. Zhang et al., proposed a novel piecewise local affine registration algorithm to register tensor images using finite strain reorientation [97]. The tensor image is divided into uniform regions and transform each region affinely. The rotation component is explicitly optimized for improving the registration. The pieces are then fused together and a smooth warp field is generated. The drawback of this method is that it does not take into consideration any structural marker and it is unclear if any optimality is lost in fusing the transformations [95]. Verma and Davatzikos [85] proposed a multichannel characterization of the diffusion data at a voxel to facilitate correspondence detection, where the features are obtained by applying a novel Gabor filter.

Park et al. [65] further examined Guimonds multi-channel method and find instead that the use of all tensor components together with PPD reorientation yields the most reliable registration results. The different combination of channels that was included for the registration of real and synthetic diffusion data was: T2-weighted intensity alone; fractional anisotropy alone; difference of the first and second tensor eigenvalues; fractional anisotropy together with trace of the tensor; all three tensor eigenvalues; and the 6 independent tensor components.

In this thesis, a novel multichannel registration based on non-parametric diffeomorphic image registration coupled with demons algorithm is proposed. Our approach concentrates on alignment of gray matter areas using the T1-weighted image and white matter using the tensor information generated from the diffusion weighted images. Section 2.2 describes the complete procedure used for registration of the ten-

sors. The registration procedure that we implemented has two advantages over the registration proposed by Park et al. Firstly, we include T1-weighted data along with the tensors. During the registration the contribution from each channel is defined by the FA threshold. This gives a morphological indication while matching the tensors. Secondly, since we use the diffeomorphic demons registration [84] the update vector field is constrained to be diffeomorphic. The difference can be observed through the tensor overlap results. Section 3.2 shows the results using multichannel diffeomorphic demons registration. The average overlap for 4 subjects is around 0.8 compared to the results by Park et al., where the overlap is approximately 0.65.

While using multichannel registration, our framework is generalized such that it can accommodate more channels or a combination of different channels. Other scalar indices like FA, trace, RA, eigenvalues etc. can be used along with the tensor components. The limitation of multichannel registration with tensor reorientation performed at each iteration is that it can be time consuming. A way around is to perform only T1-weighted registration in the first two resolution levels and then include all the channels in the final resolution level.

Curran and Alexander developed a method in which the tensor rotation component was optimized as well [27]. By using a synthetic data it was demonstrated that the tensor matching improved. In the future we would like to include the reorientation parameter in computation of the gradient.

Finally, we have applied the spatial normalization method for a population study. 9 controls and 9 patients with Schizophrenia were chosen for the study. One of

the subjects was chosen as the template image. The multistage registration framework described in section 2.2 was applied to all the subjects.

Tensor analysis is a complicated problem since the tensors do not lie in a vector space. Therefore it is not as straight forward as applying usual euclidean methods for performing analysis. Groups like Fletcher et al., Pennac et al. discovered that tensors lie on a non-linear manifold called as the Reimannian manifold [30], [67]. Tensor average, interpolation and hypothesis testing can be performed on the manifold. Although the results are accurate, this method is computationally expensive. Asigny et al. showed that instead a log-euclidean manifold can be used with equal accuracy and less computations [8].

Here we implemented the log-euclidean method developed by Arsigny on a control and patient group. The regression analysis in log-euclidean space was performed as described in section 2.3.2.1 [55]. Results show that there is a significant difference in the anisotropy in the anterior regions of the brain that include the areas near the ventricles, superior corona radiata, forceps minor, anterior limb of the internal capsule and genu of the corpus callosum.

The results were verified by implementing voxel-wise analysis on FA images and GA images. The FA analysis did not show as many significant areas as the tensor analysis, the change was significantly observed in frontal areas of the brain. A reduction in FA was observed in the patients in the genu of the corpus callosum and the forceps minor. Significant differences in the anisotropy were observed using GA analysis. The regions include parts of genu and splenium of corpus callosum, anterior

corona radiata and forceps minor.

A lot of studies that involve group analysis between control and schizophrenia patients have been performed in the recent past. Some groups like Buchsbaum et al., Wolkin et al., have reported similar findings i.e. changes in anisotropy in the anterior regions of brain [18], [92] and FA reduction has been observed in the anterior cingulum by Wang et al., and Sun et al. [88], [77]. Changes in the sub-cortical regions like white matter around thalamus were reported by Andreasen et al., based on T1-weighted data [6]. Research groups like Burns et al., Kubicki et al., found out that there was white matter disruption in the uncinate fasciculus leading to the conclusion that a fronto-temporal disconnectivity existed in patients with schizophrenia [19], [46].

Other groups have observed that the reduction in FA is mostly in the posterior parts of the brain. For example, Foong et al. and Agartz et al., observed a change in the FA values in the splenium of the corpus callosum but did not see any changes in the genu of the corpus callosum [31], [1]. Lim et al., found that schizophrenic patients exhibited widespread lower FA in the white matter, extending from frontal to occipital areas [57]. The variation in results may be due to the sample size used and the methodology implemented for the analysis.

We have verified that the results from tensor analysis with FA and GA analysis. Although there is a lot of variation in the results from the comparative methods, some regions like the parts of forceps minor were found to be significant using all three types of analyses. The difference between these methods could be the result of more sensitivity of the tensor as a response function or GA being a hyperbolic tangent

function when compared with FA. There's not enough study from which one can know how much sensitive tensor analysis could be when compared with the standard FA analysis between groups. There is still scope for research that compares results from different analyses. Also various tensor analysis methods like log-euclidean and Reimannian methods should be compared between each other using a particular group of patients and controls.

CHAPTER 5
CONCLUSION

In this thesis, a novel spatial normalization technique for diffusion tensors has been proposed. Tensor analysis between groups has been performed using the log-euclidean method.

In the first part the framework for gradient rotation method is described. The framework is such that it can be used for tensors as well as higher order models like q-ball data and high order tensors. Using the gradient rotation method, eliminates the complex problem of tensor interpolation that is under research for a decade.

In the second part, a multistage registration scheme for spatial normalization of tensors is described. The intersubject registration is carried out using multiple channels. The contribution from each channel is defined by the FA threshold. Using T1-weighted data with the tensors, helps in aliging the white matter regions as well as the gray matter regions.

In the last part a population study between controls and Schizophrenic patients is performed. The analysis is performed by converting the tensors to log-euclidean space. Our findings suggest an overall reduction in white matter organization, the deficits appear to be greater in the anterior portion of the brain than the posterior part.

The potential of this package is such that it can be used for population studies that involve hundreds of control and patient data. Different types of disorders

like Alzeimers, multiple sclerosis, huntington's disease etc. can be can be analysed using the proposed method. Although the method is not too complicated and the computation time is moderate, the output is decent.

Future work involves applying the multi-channel registration to q-ball volumes and include gradient rotation in the registration. Studying the sensitivity of different tensor analyses methods is required.

REFERENCES

[1] I Agartz, J Anderrson, and S Skare. Abnormal brain white matter in schizophrenia: a diffusion tensor imaging study. *Neuroreport*, 12(10):2251–2254, 2001.

[2] AL Alexander and Tsuruda JS. Elimination of eddy current arifacts in diffusion weighted echo planar images: the use of bipolar gradients. *Magnetic Resonance in Medicine*, 38:1016–1021, 1997.

[3] D C Alexander, JC Gee, and R Bajcsy. Elastic matching of diffusion tensor magnetic resonance images. *IEEE Computer Vision and Pattern Recognition*, 1:249, 1999.

[4] D C Alexander, C Pierpaoli, PJ Basser, and JC Gee. Spatial transformations of diffusion tensor magnetic resonance images. *IEEE Transactions On Medical Imaging*, 20(11):1131–1139, 2001.

[5] DC Alexander. *An Introduction to Computational Diffusion MRI: the Diffusion Tensor and Beyond*. Springer, Berlin Heidelberg, 2006.

[6] N Andreasen, S Arndt, V Swayze, T Cizadlo, M Flaum, D O'Leary, J Ehrhardt, , and W Yuh. Thalamic abnormalities in schizophrenia visualized through magnetic resonance image averaging. *Science*, 266(5183):294–298, 1994.

[7] B Ardekani, J Nierenberg, Matthew Hoptman, Daniel Javitt, and Kelvin Lim. Mri study of white matter diffusion anisotropy in schizophrenia. *Neuroreport*, 14(16):2025–2029, 2003.

[8] V Arsigny, P Fillard, X Pennac, and N Ayache. Log-euclidean metrices for fast and simple calculus on diffusion tensors. *Magnetic Resonance in Medicine*, 56(2):411–421, 2006.

[9] Axer. *Why is the study of brain white matter tracts important and how can it be done?* Jena Germany, 2005.

[10] P Barzo, A Marmarou, P Fatouros, K Hayasaki, and F Corwin. Contribution of vasogenic and cellular edema to traumatic brain swelling measured by diffusion-weighted imaging. *J Neurosurgery*, 87:900–907, 1997.

[11] P Basser and D Jones. Diffusion tensor mri: Theory, experimental design and data analysis - a technical review. *NMR in Biomedicine*, 15:456–457, 2002.

[12] P Basser and S Pajevic. Statistical artifacts in diffusion tensor mri (dt-mri) caused by background noise. *Magn. Resonance in Imaging*, 44:41–50, 2000.

[13] P Batchelor, M Moakher, D Atkinson, F Calamante, and A Connelly. A rigourous framework for diffusion tensor calculus. *Magnetic Resonance in Medicine*, 3749:115–122, 2005.

[14] TE Behrens, H Johansen-Berg, MW Woolrich, SM Smith, CA Wheeler-Kingshott, PA Boulby, GJ Barker, EL Sillery, K Sheehan, O Ciccarelli, AJ Thompson, JM Brady, and PM. Matthews. Non-invasive mapping of connections between human thalamus and cortex using diffusion imaging. *Nat Neuroscience*, 6(7):750–757, 2003.

[15] H Berg. *Random Walks in Biology*. Princeton University Press, Princeton, 1983.

[16] R Bishop and S Goldberg. *Tensor Analysis on Manifolds*. Dover Publications, New York, 1980.

[17] RS Briellmann, LA Mitchell, AB Waites, DF Abbott, GS Pell, MM Saling, and GD Jackson. Correlation between language organization and diffusion tensor abnormalities in refractory partial epilepsy. *Epilepsia*, 44(12):1541–1555, 2003.

[18] M Buchsbaum, J. Friedman, K Buchsbaum, B Chu, E Hazlett, R Newmark, J Schneiderman, C Torosjan, Y Tang, and P Hof. Diffusion tensor imaging in schizophrenia. *Biological Psychiatry*, 60(11):1181–1187, 1996.

[19] J Burns, M Bastin, H Whalley, T Macgillivray, and E Johnstone. Structural disconnectivity in schizophrenia: a diffusion tensor magnetic resonance imaging study. *British Journal of Psychiatry*, 182, 2003.

[20] Y Cao, M Miller, S Mori, R Winslow, and L Younes. Diffeomorphic matching of diffusion tensor images. *Proceedings of Workshop on Mathematical methods in biomedical image analysis, international conference on computer vision and pattern recognition*, 2006.

[21] H Chabriat, K Vahedi, and CA Clark. Decreased hemispheric water mobility in hemiplegic migraine related to mutation of cacna1a gene. *Neurology*, 54:510–512, 2000.

[22] L Chang and T Ernst. Mr spectroscopy and diffusion-weighted mr imaging in focal brain lesions in aids. *Neuroimaging Clin N Am*, 7:409–426, 1997.

[23] P Cheng, VA Magnotta, D Wu, P Nopoulos, DJ Moser, J Paulsen, R Jorge, and NC Andreasen. Evaluation of the gtract diffusion tensor tractography algorithm: a validation and reliability study. *Neuroimage*, 31(3):1075–1085, 2006.

[24] Ming-Chang Chiang and A.D. et al. Leow. Fluid registration of diffusion tensor images using information theory. *IEEE Transactions on Medical Imaging*, 27(4):442–456, 2008.

[25] O Ciccarelli and AT Toosy. Diffusion tractography based group mapping of major white-matter pathways in the human brain. *Neuroimage*, 19(4):1545–1555, 2003.

[26] P Cook and H Zhang. An automated approach to connectivity-based partitioning of brain structures. *MICCAI*, pages 164–171, 2005.

[27] K Curran and D C Alexander. Orientation matching for registration of diffusion tensor images. *In proceddings of SPIE medical imaging*, 2003.

[28] A Field and AL Alexander. Diffusion tensor imaging in cerebral tumor diagnosis and therapy. *Top. Magn. Resonance Imaging*, 15(5):315–324, 2004.

[29] PT Fletcher and S Joshi. Riemannian geometry for the statistical analysis of diffusion tensor data. In *Proc. of CVAMIA and MMBIA Workshops*, pages 87–98, 2004.

[30] T Fletcher and S Joshi. Principal geodesic analysis on symmetric spaces: statistics on diffusion tensors. *In proceedings of CVAMIA and MMBIA workshops*, 2004.

[31] J Foong, M Maier, C Clark, G Barker, D H Miller, and D H Ron. Neuropathological abnormalities of the corpus callosum in schizophrenia: a diffusion tensor imaging study. *J Neurol Neurosurg Psychiatry*, 68(Feb):242–244, 2000.

[32] K Friston. Functional and effective connectivity in neuroimaging -a syntesis. *Human Brain Mapping*, 2(1-2):56–78, 1994.

[33] J Gee and D Alexander. Diffusion tensor image registration. *Visualization and processing of tensor fields*, 2005.

[34] H Gray, PL Williams, and LH Bannister. *Gray's Anatomy: The anatomical basis of medicine and surgery.* Elsevie, Espana, 1995.

[35] a Guimond, CG Guttmann, S Warfield, and CF Westin. Deformable registration of dt-mri data based on transformation invariant tensor characteristics. *ISBI*, 2002.

[36] J Honark. *Basics of MRI*. Rochester Institute of Technology, New York, 1997.

[37] B Horwitz. The elusive concept of brain connectivity. *Neuroimage*, 19(2):466–470, 2003.

[38] P Jezzard and S Smith. *Functional MRI - an introduction to methods*. Oxford University Press, New York, 2003.

[39] D Jones, L Griffin, D Alexander, M Catini, M Horsfield, R Howard, and SCR Willams. Spatial normalization and averaging of diffusion tensor mri data sets. *Neuroimage*, 17:592–617, 2002.

[40] DK Jones, D Lythgoe, and M Horsfield. Characterization of white matter damage in ischemic leukoaraiosis with diffusion tensor mri. *Stroke*, 30:393–397, 1999.

[41] J Kim, M Ingalhalikar, VA Magnotta, and AL Alexander. A simple method for odf reorientation after deformable imaging registration. In *ISMRM Electronic Poster*, page 3374, 2008.

[42] J Kim, M Ingalhalikar, VA Magnotta, and AL Alexander. A simple method for odf reorientation after deformable imaging registration. In *ISMRM Electronic Poster*, page 3374, 2008.

[43] T Klingberg, M Hedehus, and E Temple. Microstructure of temporo- parietal white matter as a basis for reading ability: evidence from diffusion tensor magnetic resonance imaging. *Neuron*, 25:493–500, 2000.

[44] K Krabbe, P Gideon, and P Wagn. Mr diffusion imaging of human intracranial tumours. *Neuroradiology*, 39:483–489, 1997.

[45] M Kubicki, HM Parka, CF Westin, PG Nestor, RV Mulkern, SE Maier, M Niznikiewicz, EE Connor, JJ Levitt, M Frumin, R Kikinis, FA Jolesz, RW McCarley, and ME Shenton. Dti and mtr abnormalities in schizophrenia: Analysis of white matter integrity. *Neuroimage*, 26(4):1109–1118, 2005.

[46] M Kubicki, HM Parka, CF Westin, PG Nestor, RV Mulkern, SE Maier, M Niznikiewicz, EE Connor, JJ Levitt, M Frumin, R Kikinis, FA Jolesz, RW McCarley, and ME Shenton. Dti and mtr abnormalities in schizophrenia: Analysis of white matter integrity. *Neuroimage*, 26(4):1109–1118, 2005.

[47] PC Lauterber. Image formation by induced local interactions: examples employing nuclear magnetic resonance. *Nature*, 1973.

[48] M Lazar and DM Weinstein. White matter tractography using diffusion tensor deflection. *Human Brain Mapping*, 18(4):306–321, 2003.

[49] Denis Le Bihan, Jean-Franois Mangin, Cyril Poupon, Chris Clark, Sabina Pappata, Nicolas Molko, and Hughes Chabriat. Diffusion tensor imaging: Concepts and applications. *J. Magnetic Resonance Imaging*, 13(4):534–546, 2001.

[50] D LeBihan and Peter van Zijl. From the diffusion coefficient to the diffusion tensor. *Magnetic Resonance in Medicine*, 15(7-8):431–434, 2002.

[51] A Lee, N Lepore, M Barysheva, Y Chou, C Brun, S Madsen, K McMohan, G Zubicarey, M Wright, M Toga, and P Thompson. Gene effects mapped using fractional and geodesic anisotropy in diffusion tensor images of 92 monzygotic and dizygotic twins. *MICCAI*, 2008.

[52] J Lee. *Reimannian Manifolds: An Introduction to curvature*. Springer, New York, 1997.

[53] A Leemans, J Sijbers, S Backer, E Vandervliet, and P Parizel. Affine coregsitration of diffusion tensor magnetic resonance images. *Advanced concepts for intelligent vision systems*, 3708:523–530, 2005.

[54] Y Li, H Zhu, Y Chen, J Ibrahim, A Hongyu, J Glimore, W Lin, and D Shen. Lstgee: Longitudinal analyses of neuroimaging data. *Proceedings of SPIE*, 2009.

[55] Y Li, H Zhu, Y Chen, J Ibrahim, A Hongyu, W Lin, C Hall, and D Shen. Radti:regression analysis of diffusion tensor images. *Proceedings of SPIE*, 2009.

[56] K Lim and M et al Hedehus. Compromised white matter tract integrity in schizophrenia inferred from diffusion tensor imaging. *Arch. General Psychiatry*, 56(4):367–374, 1996.

[57] KO Lim and SJ Choi. Reduced frontal white matter integrity in cocaine dependence: a controlled diffusion tensor imaging study. *Biological Psychiatry*, 51(11):890–895, 2001.

[58] V Magnotta, G Harris, NC Andreasen, DS O'Leary, WTC Yuh, and D Heckel. Structural mr image processing using the brains2 toolbox. *Comput. Med. Imaging Graph.*, 26(4):251–264, 2002.

[59] P Mansfield. Multi-planar image formation using nmr spin echoes. *Journal of Phys.*, 10:55–58, 1977.

[60] S Mori and BJ Crain. Three-dimensional tracking of axonal projections in the brain by magnetic resonance imaging. *Annals of Neurology*, 45(2):465–469, 1999.

[61] ME Moseley, J Kucharczyk, and J Mintorovitch. Diffusion weighted mr imaging of acute stroke: correlation with t2-weighted and magnetic susceptibility-enhanced mr imaging in cats. *AJNR*, 11:423–429, 1990.

[62] J Neil, S Shiran, and R McKinstry. Normal brain in human newborns: apparent diffusion coefficient and diffusion anisotropy measured by using diffusion tensor mr imaging. *Radiology*, 209:57–66, 1998.

[63] Christopher Nimsky and P et al Ganslandt. Preoperative and intraoperative diffusion tensor imaging-based fiber tracking in glioma surgery. *Neurosurgery*, 56(1):130–138, 2005.

[64] Jaccard P. Nouvelles recherches sur la distribution florale. *Bulletin de la Societe Vaudoise des Sciences Naturelles*, 44:223–270, 1908.

[65] H Park, M Kubicki, M Shenton, A Guimond, R McCarley, S Maier, R Kikinis, F Jolesz, and C Westin. Spatial normalization of diffusion tensor mri using multiple channels. *Neuroimage*, 20:1995–2009, 2003.

[66] GJM Parker and Wheeler-Kingshott. Estimating distributed anatomical connectivity using fast marching methods and diffusion tensor imaging. *IEEE Transactions on Medical Imaging*, 21(5), 2002.

[67] X Pennac, P Fillard, and N Ayache. A riemannanian framework for tensor computing. *International Journal of Computer Vision*, 66:41–66, 2004.

[68] C Pierpaoli and P. J Basser. Toward a quantitative assessment of diffusion anisotropy. *Magnetic Resonance in Medicine*, 36(6):893–906, 1996.

[69] C Pierpaoli, P Jezzard, P. J Basser, A Barnett, and G Di Chiro. Diffusion tensor mr imaging of human brain. *Radiology*, 201:637–648, 1996.

[70] F Rugg-Gunn and S Eriksson. Diffusion tensor imaging of cryptogenic and acquired partial epilepsies. *Brain*, 124:627–636, 2001.

[71] P Ruiz-Alzola, C Westin, S Warfield, C Alberola, S Maeir, and R Kikinis. Non-rigid registration of 3d tensor medical data. *Medical Image Analysis*, 6:143–161, 2002.

[72] PW Schaefer, FS Buonanno, RG Gonzalez, and LH Schwamm. Diffusion-weighted imaging discriminates between cytotoxic and vasogenic edema in a patient with eclampsia. *Stroke*, 28:1082–1085, 1997.

[73] RB Schwartz, RV Mulkern, H Gudbjartsson, and Jolesz F. Diffusion weighted mr imaging in hypertensive encephalopathy: clues to pathogenesis. *AJNR*, 19:859–862, 1998.

[74] J.S Shimony and A.Z et al. Snyder. The study of neural connectivity using diffusion tensor tracking. *Cortex*, 52(6):1358–1372, 2004.

[75] SM Smith and M et al. Jenkinson. Advances in functional and structural mr image analysis and implementation as fsl. *Neuroimage*, 23:508–219, 2004.

[76] E. O Stejskal and J. E Tanner. Spin diffusion measurements: spin echoes in the presence of a time-dependent field gradient. *Journal of Chem. Phys.*, 42:288–292, 1965.

[77] Z Sun, F Wang, L Cui, J Breeze, X Du, X Wang, Z Cong, H Zhang, B Li, N Hong, and D Zhang. Abnormal anterior cingulum in patients with schizophrenia: a diffusion tensor imaging study. *Neuroreport*, 14, 2003.

[78] J Talairach and P Tournox. *Coplanar Steriotaxic atlas of the human brain: 3 dimensional proportional system, an approach to cerebral imaging.* Thieme Medical Publications, 1988.

[79] Y. Tang and J. R. Nyengaard. A stereological method for estimating the total length and size of myelin fibers in human brain white matter. *Journal of Neuroscience Methods*, 73(2):193–200, 1997.

[80] JP Thirion. Image matching as a diffusion process: an analogy with maxwells demons. *Medical Image Analysis*, 2:243–260, 1998.

[81] H.C Torrey. Bloch equations with diffusion terms. *Phys. Rev.*, 104:563–565, 1956.

[82] D Tuch. Q ball imaging. *Magnetic Resonance in Medicine*, 40(1):213–215, 2004.

[83] DS Tuch, VJ Wedeen, AM Dale, JS George, and JW Belliveau. Conductivity tensor mapping of the human brain using diffusion tensor mri. In *Proc. National Academy Sciences*, pages 11697–11701, 2001.

[84] T Vercauteren, X Pennec, A Perchant, and N Ayache. Non-parametric diffeomorphic image registration with the demons algorithm. In *Proc. of MICCAI 07*, 2007.

[85] R Verma and C Davatzikos. Matching of diffusion tensor images using gabor features. *IEEE International Symposium on Biomedical Imaging*, 1:396–399, 2004.

[86] R Verma, P Khurd, and C Davatzikos. On analyzing diffusion tensor images by identifying manifold structure using isomaps. *IEEE Transactions on Medical Imaging*, 26(6):772–780, 2007.

[87] W.M Viola P, Wells III. Alignment by maximization of mutual information. In *IEEE Computer Society*, 1995.

[88] F Wang, Z Sun, L Cui, X Du, X Wang, and H Zhang. Anterior cingulum abnormalities in male patients with schizophrenia determined through diffusion tensor imaging. *American Journal of Psychiatry*, 163, 2004.

[89] S Warach, M Boska, and KMA Welsh. Pitfalls and potential of clinical diffusion-weighted mr imaging in acute stroke. *Stroke*, 28:481–482, 1997.

[90] R Watts and C Liston. Fiber tracking using magnetic resonance diffusion tensor imaging and its applications to human brain development. *Mentally Retard Dev. Disabililty Res. Rev.*, 9(3):168–177, 2003.

[91] DJ Werring, CA Clark, GJM Parker, DH Miller, AJ Thompson, and GJ Barker. A direct demonstration of both structure and function in the visual system: Combining diffusion tensor imaging with functional magnetic resonance imaging. *Neuroimage*, 9(3):352–361, 1999.

[92] A Wolkin, S Choi, S Szilagyi, M Sanfilipo, J Rotrosen, and K Lim. Inferior frontal white matter anisotropy and negative symptoms of schizophrenia: A diffusion tensor imaging study. *American Journal of Psychiatry*, 160:572–574, 2003.

[93] MW Woolrich, S Jbabdi, B Patenaude, M Chappell, S Makni, T Behrens, C Beckmann, M Jenkinson, and SM Smith. Bayesian analysis of neuroimaging data in fsl. *Neuroimage*, 45:173–186, 2009.

[94] D Xu, S Mori, D Shen, PCM van Zijl, and C Davatzikos. Spatial normalization of diffusion tensor fields. *Magnetic Resonance in Medicine*, 50:175–182, 2003.

[95] BT Yeo, T Vercauteran, P Fillard, X Pennac, P Golland, N Ayache, and O Clatz. Dti registration with exact finite strain differential. *ISBI*, 2008.

[96] H Zhang, P Yushkevich, D Alexander, and J Gee. Deformable registration of diffusion tensor mr images with explicit orientation optimization. *Medical Image Analysis*, 10:764–785, 2006.

[97] H Zhang, PA Yushkevich, and J Gee. Registration of diffusion tensor images. *IEEE Transactions on Medical Imaging*, 1:842–847, 2004.

[98] J Zhong, H Ni, Tong Zhu, Sven Ekholm, and Voyko Kavcic. Mr diffusion tensor imaging (dti) and neuropsychological testing for neuronal connectivity in alzheimer's disease (ad) patients. In *Proc. of SPIE*, pages 238–249, 2004.

[99] U Ziyan, M Sabuncu, L Donnell, and C Westin. Non-linear registration of diffusion mr based on fiber bundles. *Proceedings of MICCAI*, 4791:351–358, 2007.